



IMPLEMENTATION OF CRASH SIMULATION TECHNOLOGY TO DEVELOP COUNTERMEASURES STRATEGIES FOR OVERHEIGHT IMPACT PROTECTION SYSTEM ON CONCRETE GIRDERS

MARCH 2022
FHWA-RC-22-0003



U.S. Department of Transportation
Federal Highway Administration



Foreword

This report presents a comprehensive performance-based approach for the demand model and the design of supplemental protection beam against bridge strikes due to overheight heavy vehicles (OHV) impact. This work is important because recent surveys indicated OHV impact on bridge superstructure has been recognized as a serious problem across the country. However, there is no standard design or knowledge base on the OHV impact demand that can be used by engineers to design the protection systems for bridge girders. The effectiveness of current retrofit approaches, such as carbon-fiber reinforced polymers (CFRP) wrapping, for pre-stressed concrete girders damaged during OHV impact, has not been systematically studied.

The work reported herein evaluated the efficacy of wrapping concrete girders with CFRP for protection against significant damages due to OHV impact in detail. To minimize damage to fascia girders, installing energy-absorbing materials such as aluminum honeycombs in front of the girder or as sacrificial beam is proposed. The effectiveness and capabilities of these supplemental systems in protecting pre-stressed fascia girders of bridges were investigated through high fidelity computational simulation and large scaled drop-hammer tests. This report will be of interest to bridge program personnel from federal, state, and local agencies as well as to parties engaged in bridge-related research, and the practicing bridge engineering community. The findings and recommendations will also serve as pertinent resources to the ongoing transportation pooled fund study TPF-5(484)- Develop countermeasure strategies for protecting bridge girders against overheight vehicular impact.

Shay K. Burrows P.E.
Resource Center Director
Federal Highway Administration
Office of Innovation Implementation

Notice

This document is disseminated under the sponsorship of the U.S. Department of Transportation in the interest of information exchange. The U.S. Government assumes no liability for the use of the information contained in this document.

The U.S. Government does not endorse products or manufacturers. Trademarks or manufacturers' names appear in this report only because they are considered essential to the objective of the document.

Quality Assurance Statement

The Federal Highway Administration (FHWA) provides high-quality information to serve Government, industry, and the public in a manner that promotes public understanding. Standards and policies are used to ensure and maximize the quality, objectivity, utility, and integrity of its information. FHWA periodically reviews quality issues and adjusts its programs and processes to ensure continuous quality improvement.

TECHNICAL REPORT DOCUMENTATION PAGE

1. Report No. FHWA-RC-22-000	2. Government Accession No.	3. Recipient's Catalog No.	
4. Title and Subtitle Implementation of crash simulation technology to develop countermeasures strategies for overheight impact protection system on concrete girders		5. Report Date January 25, 2022	
7. Author(s) Agrawal, A.K., El-Tawil, S., and Cao, R.		6. Performing Organization Code:	
9. Performing Organization Name and Address The City College of New York 160 Convent Ave, New York, NY 10031		8. Performing Organization Report No.	
12. Sponsoring Agency Name and Address Office of Research, Development, and Technology Federal Highway Administration 6300 Georgetown Pike McLean, VA 22101-2296		10. Work Unit No.	
		11. Contract or Grant No. DTFH61-14-D-00010/0003	
		13. Type of Report and Period Final Report, 04/10/2019- 01/25/2021	
		14. Sponsoring Agency Code HRDI-20	
15. Supplementary Notes The Federal Highway Administration (FHWA) Study Manager was Waider Wong (FHWA).			
16. Abstract Based on the 2016 National Bridge Inventory (NBI) database available at the FHWA, there are a total of 614,387 bridges in the United States. It has been observed from previous research that collision, both caused by vessel and vehicles, is the second leading cause of bridge failures. Recently, overheight impact on bridge superstructure has been recognized as a serious problem across the country. However, there is no standard design or knowledge base on the overheight impact demand that can be used by engineers to design the protection systems for bridge girders. The effectiveness of current retrofit approaches, such as carbon-fiber reinforced polymers (CFRP) wrapping, for pre-stressed concrete girders damaged during overheight impact, has not been systematically studied. Hence, the objective of the proposed research was to use crash simulation technology for developing a comprehensive approach for the demand model and performance-based design of supplemental protection beams. The efficacy of wrapping concrete girders with CFRP for protection against significant damage by overheight impact was also evaluated in detail. To minimize damage to fascia girders, energy-absorbing materials, such as aluminium honeycombs, have been proposed to be installed in front of the girder or sacrificial beams. The effectiveness and capabilities of these supplemental systems in protecting pre-stressed fascia girders of bridges were investigated through high fidelity computational simulation and scaled drop-hammer tests.			
17. Key Words Vehicular impacts, overheight impact with bridges, impact protection		18. Distribution Statement No restrictions. This document is available to the public through the National Technical Information Service, Springfield, VA 22161. http://www.ntis.gov	
19. Security Classification (of this report) Unclassified	20. Security Classification (of this page) Unclassified	21. No. of Pages 48	22. Price

SI* (MODERN METRIC) CONVERSION FACTORS

APPROXIMATE CONVERSIONS TO SI UNITS				
Symbol	When You Know	Multiply By	To Find	Symbol
LENGTH				
in	inches	25.4	millimeters	mm
ft	feet	0.305	meters	m
yd	yards	0.914	meters	m
mi	miles	1.61	kilometers	km
AREA				
in ²	square inches	645.2	square millimeters	mm ²
ft ²	square feet	0.093	square meters	m ²
yd ²	square yard	0.836	square meters	m ²
ac	acres	0.405	hectares	ha
mi ²	square miles	2.59	square kilometers	km ²
VOLUME				
fl oz	fluid ounces	29.57	milliliters	mL
gal	gallons	3.785	liters	L
ft ³	cubic feet	0.028	cubic meters	m ³
yd ³	cubic yards	0.765	cubic meters	m ³
NOTE: volumes greater than 1000 L shall be shown in m ³				
MASS				
oz	ounces	28.35	grams	g
lb	pounds	0.454	kilograms	kg
T	short tons (2000 lb)	0.907	megagrams (or "metric ton")	Mg (or "t")
TEMPERATURE (exact degrees)				
°F	Fahrenheit	5 (F-32)/9 or (F-32)/1.8	Celsius	°C
ILLUMINATION				
fc	foot-candles	10.76	lux	lx
fl	foot-Lamberts	3.426	candela/m ²	cd/m ²
FORCE and PRESSURE or STRESS				
lbf	poundforce	4.45	newtons	N
lbf/in ²	poundforce per square inch	6.89	kilopascals	kPa
APPROXIMATE CONVERSIONS FROM SI UNITS				
Symbol	When You Know	Multiply By	To Find	Symbol
LENGTH				
mm	millimeters	0.039	inches	in
m	meters	3.28	feet	ft
m	meters	1.09	yards	yd
km	kilometers	0.621	miles	mi
AREA				
mm ²	square millimeters	0.0016	square inches	in ²
m ²	square meters	10.764	square feet	ft ²
m ²	square meters	1.195	square yards	yd ²
ha	hectares	2.47	acres	ac
km ²	square kilometers	0.386	square miles	mi ²
VOLUME				
mL	milliliters	0.034	fluid ounces	fl oz
L	liters	0.264	gallons	gal
m ³	cubic meters	35.314	cubic feet	ft ³
m ³	cubic meters	1.307	cubic yards	yd ³
MASS				
g	grams	0.035	ounces	oz
kg	kilograms	2.202	pounds	lb
Mg (or "t")	megagrams (or "metric ton")	1.103	short tons (2000 lb)	T
TEMPERATURE (exact degrees)				
°C	Celsius	1.8C+32	Fahrenheit	°F
ILLUMINATION				
lx	lux	0.0929	foot-candles	fc
cd/m ²	candela/m ²	0.2919	foot-Lamberts	fl
FORCE and PRESSURE or STRESS				
N	newtons	0.225	poundforce	lbf
kPa	kilopascals	0.145	poundforce per square inch	lbf/in ²

* SI is the symbol for the International System of Units. Appropriate rounding should be made to comply with Section 4 of ASTM E380. (Revised March 2003)

TABLE OF CONTENTS

CHAPTER 1. INTRODUCTION	1
Background	1
Objectives.....	3
CHAPTER 2. DEVELOPMENT OF A SUPPLEMENTAL PROTECTIVE SYSTEM FOR OVERHEIGHT IMPACT	5
Hazard Level Comparison	8
Material Model.....	8
Validation.....	8
Simulation Results	9
Parametric Studies.....	10
Simplified Pulse Model For Overheight Impact	12
Performance-Based Design	14
Proposed Design Procedure	16
Validation Of The Proposed Framework	17
CHAPTER 3. RETROFIT OF GIRDERS DAMAGE DURING OVERHEIGHT IMPACT USING CARBON-FIBER REINFORCED POLYMERS	18
MODEL OF THE TRUCK AND BRIDGE.....	18
Bridge Model	18
Material Model.....	19
Simulation Results	20
Parametric Study	21
Pushover Analysis Simulation	23
CHAPTER 4. OVERHEIGHT IMPACT ON GIRDERS WITH HONEYCOMB LAYERS	26
Energy Method for Honeycomb Device Design	26
Validation of the Honeycomb Modeling	26
Truck Impact Simulation	27
CHAPTER 5. LARGE SCALE TESTING OF A GIRDER WITH HONECOMB BLOCK	31
CHAPTER 6. CONCLUSIONS, LIMITATIONS AND FUTURE WORK	38
Summary and Conclusions	38
Limitations and Future Work.....	38
REFERENCES.....	40

LIST OF FIGURES

Figure 1. Chart. Causes of bridge failures in the United States.....	1
Figure 2. Map. Number and seriousness of bridge hits problem in the United States during 2005-2008.....	2
Figure 3. Graph. Types of overheight vehicles impacting bridge superstructures in New York State.....	2
Figure 4. Drawing. Installation of overheight protection beams on a bridge.	3
Figure 5. Photo. Original tractor-semitrailer model.....	5
Figure 6. Photo. Collapse scene of the Skagit River bridge.	6
Figure 7. Photo. Damage mode of the trailer in the Skagit river bridge collapse.....	6
Figure 8. Photo. Simulation setup of overheight impact with Skagit River bridge in LS-DYNA.	7
Figure 9. Photo. Progress of the impact and damage mode of the trailer after impact.....	7
Figure 10. Photo. Comparison of the collapse scenario between the accident and FE simulation in LS-DYNA.	7
Figure 11. Photo. Example concrete bridge model subject to the modified semi-rigid trailer impact.....	9
Figure 12. Photo. Typical severe damage mode of the concrete girder subject to semi-rigid trailer impact.....	9
Figure 13. Photo. Typical minor damage mode of the concrete girder subject to normal trailer impact.....	10
Figure 14. Photo. Simulation setup of overheight impact with steel box beam.	11
Figure 15. Graph. Impact responses for steel beams with truck weight of 20 tons.....	11
Figure 16. Graph. Impact responses for steel beams with truck speed of V70.....	12
Figure 17. Graph. Simplified triangle pulse loading model.....	12
Figure 18. Illustration. Loading application of the pulse model.....	13
Figure 19. Graph. Comparison of the beam displacement caused by the truck impact and pulse loading.....	14
Figure 20. Graph. Capacity calculation model for steel box beams.	15
Figure 21. Graph. Performance based design chart for the steel box beam.....	16
Figure 22. Photo. Example concrete bridge model subject to the modified semi-rigid trailer impact.....	18
Figure 23. Photo. Example prestressed concrete bridge.....	19
Figure 24. Illustration. Illustration of CFRP wrapping on prestressed concrete girders.	19
Figure 25. Photo. Typical damage mode of the CFRP wrapped girders subject to overheight impact from actual accidents and simulations.	20
Figure 26. Photo. Localized damage of the CFRP wrapping from the simulation.	21
Figure 27. Graph. Effects of CFRP on the girder deformations subject to overheight impact (V55-W40).	21
Figure 28. Graph. Deformation of the CFRP wrapped girder subject to different truck impact. .	22
Figure 29. Graph. Impact force time history for a 40-ton truck at different speeds.	22
Figure 30. Photo. Damage mode of the CFRP wrapped girder.	23
Figure 31. Illustration. Pushover loading setup on the concrete girder.	24
Figure 32. Graph. Pushover curve from the simulation.....	24
Figure 33. Graph. Patterns of the yield lines of concrete girder under pushover loading.	25
Figure 34. Illustration. Illustration of the yield line method.....	25

Figure 35. Photo. Simulation setup of pushover on the honeycomb sample.....	27
Figure 36. Graph. Pushover curves of the honeycomb.....	27
Figure 37. Photo. Simulation setup of honeycomb modular subject to the overheight impact. ...	28
Figure 38. Graph. Crushing behavior of the honeycomb.....	28
Figure 39. Graph. Impact force time history of the honeycomb beam subject to the overheight impact.....	29
Figure 40. Graph. Comparison of peak deformation of the girder protected by CFRP and honeycomb blocks.	30
Figure 41. Photo. Minor damage mode of bridge girder protected by the honeycomb modular..	30
Figure 42. Photo. Setup of the drop-hammer test.	31
Figure 43. Illustration. Two configurations of the honeycomb.	32
Figure 44. Photo. Impact process of the 20-mph case.	33
Figure 45. Graph. Deformation time history of the beam under the 20-mph drop-hammer impact.	34
Figure 46. Graph. Impact force time history of the 20-mph drop hammer impact.....	34
Figure 47. Graph. Deformation time history of the beam under the 10-mph drop-hammer impact.	35
Figure 48. Graph. Impact force time history of the 10-mph drop-hammer impact.	35
Figure 49. Graph. Damage mode of the beam under 20-mph drop-hammer impact.....	36
Figure 50. Graph. Deformation mode of the beam under 10-mph drop-hammer impact.....	36
Figure 51. Graph. Strain of the beam at point A (in figure 42).	37

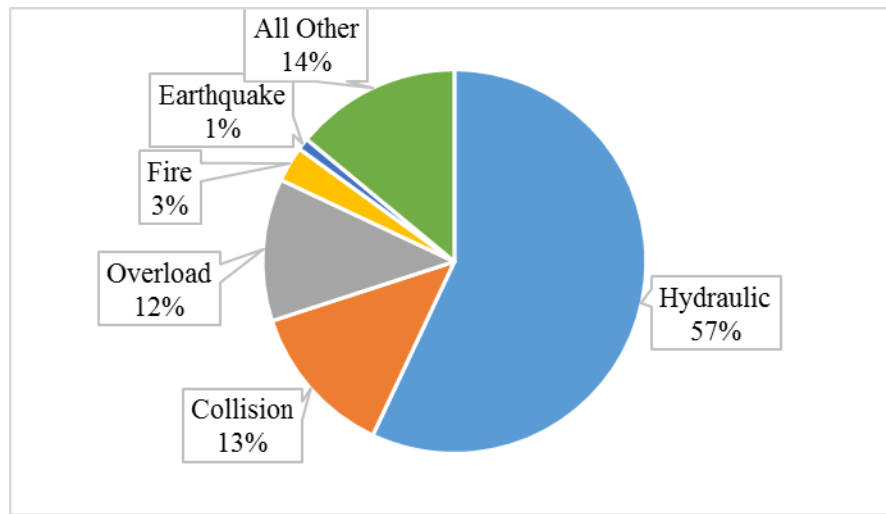
LIST OF TABLES

Table 1. Comparison of calibrated pulse demands in FEM and proposed equation results	14
Table 2. Computed ductility ratio for the impact beams subject to truck impact	16
Table 3. Performance levels, corresponding damage state, and rotation.....	16
Table 4. Beam geometry for validation study.....	17
Table 5. Selected cases for validation of proposed method.....	17
Table 6. Computed energy of the trailer and honeycombs	30
Table 7. Displacement results for each testing case	32

CHAPTER 1. INTRODUCTION

BACKGROUND

Based on the 2016 National Bridge Inventory database available at the FHWA¹, there are a total of 614,387 bridges in the United States. The National Highway Traffic Safety Administration (NHTSA) estimates that annually 1,000 trucks and buses with gross weight greater than 10,000 pounds collide with bridge structures (Zimmerman 2012). Based on bridge failure data compiled by the New York State Department of Transportation, Figure 1 shows the leading causes of bridge failures in the United States during 1969 to 2006. It is observed that collision, both caused by vessel and vehicles, has been recognized as the second leading cause of bridge failures after hydraulic failures.

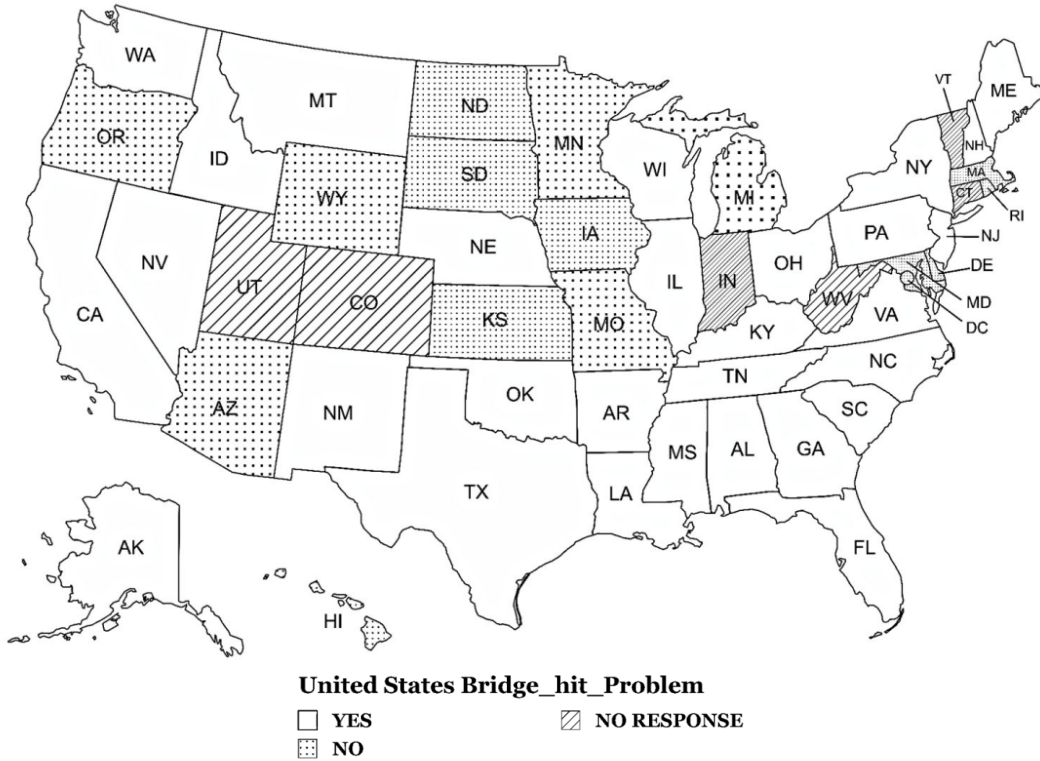


Source: FHWA

Figure 1. Chart. Causes of bridge failures in the United States.

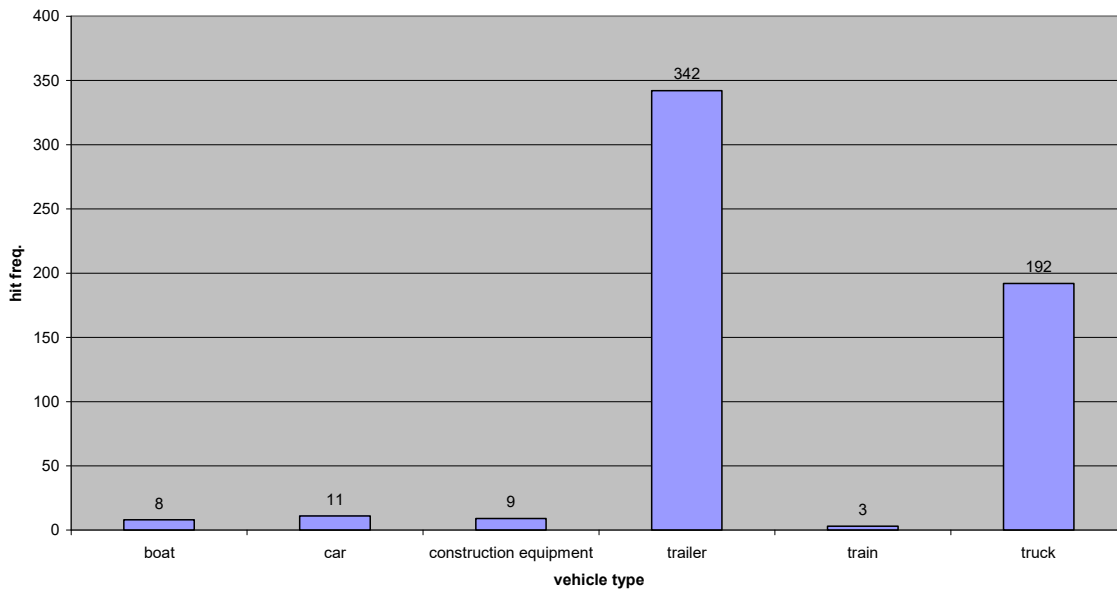
A recent study by Agrawal et al. (2011) has shown the impact of overweight trucks on bridge superstructure is a “high likelihood” event that causes damages to steel or concrete components of bridges and creates significant traffic congestion in the aftermath of the impact. The survey by Agrawal et al. (2011) in figure 2 asked the States whether the impact of bridges is a serious problem in the United States. It is observed that the overweight impact on bridge superstructure has generally been considered as a serious problem across the country. It should also be noted that the number of impacts for the period of 2005-2008 shown in figure 2 might not directly show the seriousness of the impact. For example, Missouri had many impacts (1,691). However, most hits resulted in minor damages or scratches on bridges. Therefore, Missouri considered bridge impacts a minor problem. Also, Virginia data had been updated based on recent information. Based on the analysis of data from the New York State Department of Transportation (NYSDOT) on impacts by overweight vehicles, figure 3 shows that tractor-semitrailers were impacting bridge superstructures the most frequently.

¹ <https://www.fhwa.dot.gov/bridge/nbi/ascii.cfm>



Source: NYSDOT

Figure 2. Map. Number and seriousness of bridge hits problem in the United States during 2005-2008.

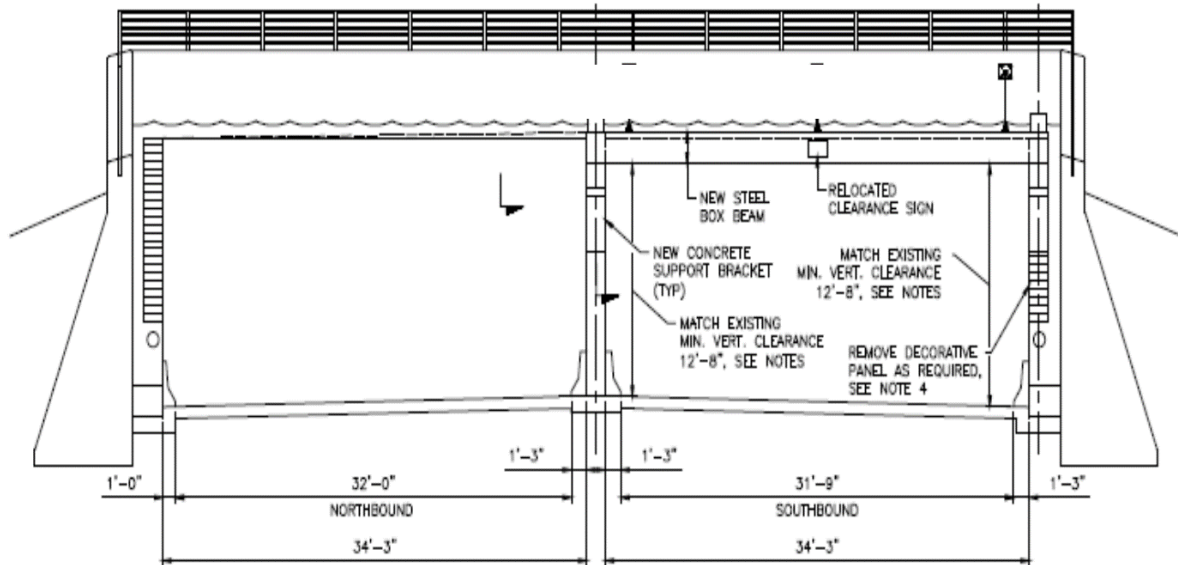


Source: NYSDOT

Figure 3. Graph. Types of overweight vehicles impacting bridge superstructures in New York State.

Although most of the States use a detection system to warn overweight trucks from impacting bridge superstructure, the superstructure/tunnels could still be damaged if the driver does not

follow the warning signs, or the detention systems malfunctions. In such cases, some States install protection beams at the entrance of bridges/tunnels. These protection beams are designed as a supplemental structure to prevent overheight portions of trucks from impacting fascia girders of the bridges or for preventing overheight trucks from entering a tunnel. Figure 4 shows an example of such a system installed at the entrance of a bridge. The design of such protection beams was based on approximate impact analysis. Currently, there is no standard design or knowledge base on impact force demand that can be used by engineers to design the protection beam. Qiao et al. (2008) conducted simulations and testing on FRP sandwich as overheight impact protection system, did not provide a demand model for impacting tractor-semitrailers. Hence, further studies are needed to develop a demand model of overheight impact for the design of impact protection systems. Based on such demand model, a supplemental system (such as a protection beam) could be designed to prevent any significant damage to the fascia girder of bridges. This protection beam could be replaced after any impact event if it suffered any damage. It has been recognized by State DOT engineers that pre-stressed concrete girders are at an increased risk of failure due to overheight impact, which can be prevented by installing such protection systems. Hence, the main objective of the proposed research is to develop a comprehensive approach for the demand model and performance-based design of protection beams for bridges at risk of impacts by overheight trucks.



Source: NYCDOT

Figure 4. Drawing. Installation of overheight protection beams on a bridge.

OBJECTIVES

The Federal Highway Administration (FHWA) has recently developed a technology for crash simulation using the enhanced non-linear finite element model of the tractor-trailer as well as the single unit truck (SUT) in LS-DYNA. This technology is being used extensively for investigating the safety of bridge piers for frontal impact by heavy trucks as well as side collisions on superstructure due to overheight vehicles. The main objective of this research is to use this technology for developing a comprehensive approach for the demand model and performance-based design of supplemental protection beams. These protection beams have also been made of

energy-absorbing materials, such as aluminum honeycombs, to minimize damage to fascia girders in the event of overheight trucks moving at high speeds. The efficacy of wrapping concrete girders with carbon-fiber-reinforced polymers (CFRP) for protection against overheight impact has also been evaluated through high-fidelity truck collision simulations. Based on the simulation results, the effectiveness, and capabilities of these supplemental systems in protecting pre-stressed fascia girders of bridges were investigated in detail. These objectives of this research have been achieved through the following eight tasks.

- Task 1: Conceptual development of a supplemental protective system for overheight impact.
- Task 2: Literature search and data collection on Carbon Fiber Reinforced Polymers(CFRP) wrapping protection for overheight impact.
- Task 3: Modeling replaceable aluminum honeycombs filled with energy-dissipative materials.
- Task 4: Simulating overheight impact on the protection devices installed on the pre-stressed girders.
- Task 5: Material behavior and damage mechanisms of the honeycomb through laboratory testing.
- Task 6: Design of field test setup through numerical simulations.
- Task 7. Scaled impact testing on the honeycomb devices.
- Task 8. Theoretical verifications with test results.

Detailed work performed towards achieving these eight tasks is described in different chapters of this report as follows:

Chapter 2 describes the development of a supplemental protection system for overheight impact, including the demand model and the performance-based design framework.

Chapter 3 describes survey results of CFRP usage among state DOTs for protecting concrete girders against overheight impact and other retrofits. Simulation results have also been presented to evaluate the effectiveness of the CFRP wrapping on the impact performance of the pre-stressed concrete girders subject to truck impact.

Chapter 4 describes the modeling of honeycomb materials and presents simulation results of truck collisions with honeycomb beams installed on a full-scale bridge model. A simple design method of the honeycomb beam was also proposed for engineer use in a practical setting. The efficacy of honeycomb beams was compared with the CFRP wrapping for protecting pre-stressed concrete girders against overheight truck impact.

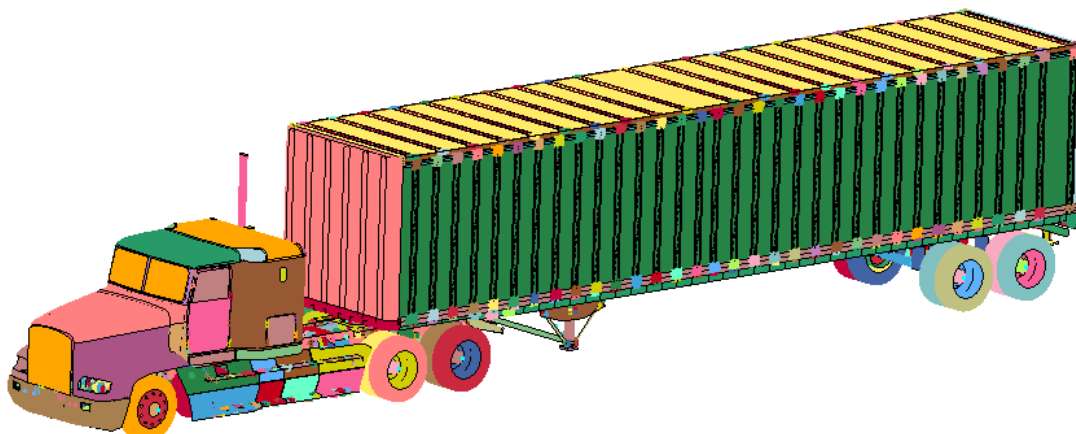
Chapter 5 presents the testing results of drop-hammer impact with steel beams installed with honeycombs. Simulation verification is also presented in this chapter.

Chapter 6 presents conclusions and recommendations for future work.

CHAPTER 2. DEVELOPMENT OF A SUPPLEMENTAL PROTECTIVE SYSTEM FOR OVERHEIGHT IMPACT

An advanced tractor-semitrailer model developed recently by the Federal Highway Administration and used extensively by the authors was further modified for developing a demand model of overheight impact for the design of impact protection systems. Figure 5 shows the truck model used in the simulations. The truck model was originally developed by the National Crash Analysis Center (NCAC) and updated by Battelle (Plaxico et al. 2008). The trailer model was developed at Battelle and the overall model was validated against several full-scale barrier impact tests (Plaxico et al. 2009 and Miele et al. 2010). The truck model is a van-type tractor-semitrailer with dimensions of 66 ft x 9 ft x 13 ft and is representative of models such as 1991 White GMC tractor with a 1988 Pines 14.6-m semitrailer, 1979 International TranStar 4200 tractor with a 1977 Pullman van-trailer and 1992 Freightliner FLD120 with integral sleeper cabin or a 1990 Stoughton box semitrailer (Miele et al. 2010). The finite element model of the truck is composed of approximately 472,000 finite elements, including shell, beam, and solid elements for different parts of the truck. This model has also been used for hundreds of simulations for cases within the scope of TL-5 speeds and impact angles in NCHRP Report 350 (Ross et al. 1993) and has been shown to be reasonably representative and accurate (Agrawal et al. 2018). Further details about this model can be found in Miele et al. (2010) and at the National Transportation Research Center website (<https://thyme.ornl.gov/fhwa/tractortrailer/>).

In the original trailer model, the trailer body was comprised of roof and side panels that were light and were mostly constructed of thin plywood, aluminum, and steel sheets. Therefore, the original trailer's main body was not strong or stiff enough to represent a severe overheight impact hazard. For example, figure 6 shows a steel truss bridge over the Skagit River near Mount Vernon, Washington, that collapsed due to the overheight impact. Figure 7 shows that the impacting trailer carried a special cargo comprised of a heavily reinforced container-like structure without side panels. The trailer behaved mostly as a rigid body during the impact, as evinced by the presence of minor damage in the trailer's top part. Hence, the original trailer model shown in figure 5 was modified to be more rigid (adjusting material strength and thickness) and it was calibrated against the damage mode of the semi-rigid trailer in the Skagit River bridge collapse.



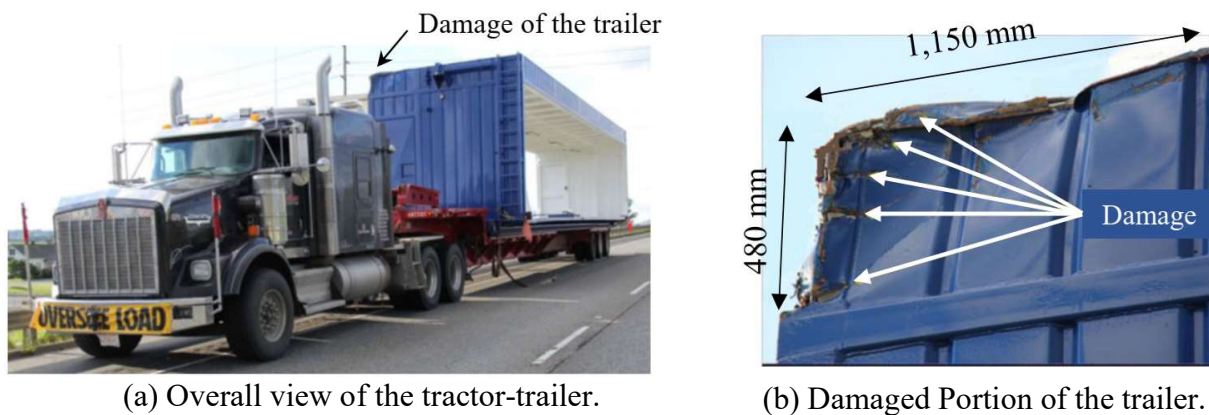
Source: FHWA

Figure 5. Photo. Original tractor-semitrailer model.



Source: NTSB

Figure 6. Photo. Collapse scene of the Skagit River bridge.



(a) Overall view of the tractor-trailer.

(b) Damaged Portion of the trailer.

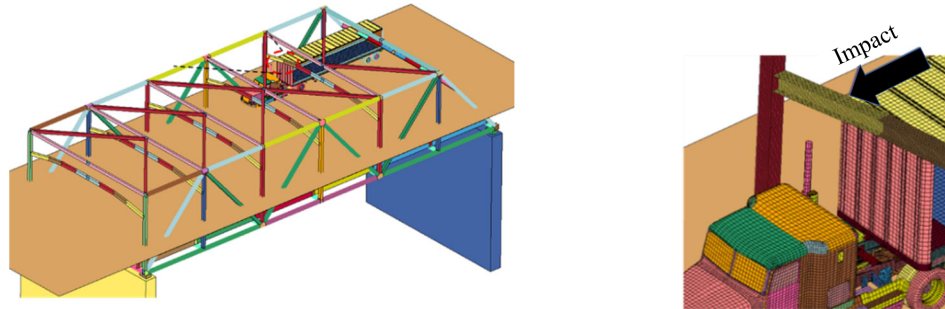
Source: NTSB

Figure 7. Photo. Damage mode of the trailer in the Skagit river bridge collapse.

Based on the as-built drawings, figure 8 shows the simulation setup of the overheight impact with the Skagit River bridge model in LS-DYNA (Hallquist 2006). The main trusses of the bridge were modeled using shell elements. The truss members were connected to the gusset plates using the nodal rigid body command in LS-DYNA (Hallquist 2006). This implies that connection failure was not permitted to occur, which is consistent with field observations after the incident. The mesh size of the bridge superstructure was 1.5 inch. The piers were modeled using rigid materials and fully fixed at the bottom. The total number of elements in the model was approximately 1.1 million. Plastic kinematic material (Mat 3) in LS-DYNA (Hallquist 2006) was used to model the steel members, with a failure strain of 0.2. The yielding strength of the steel was assumed to be 50 ksi based on the design drawings. More detailed information of the bridge model can be found in Cao et al. (2020a).

Based on the calibration, figure 9 shows the damage mode of the calibrated trailer model after the impact. It can be seen from figure 9 that the trailer corner suffered localized damage, the area and location of which matched the damage in the actual trailer shown in figure 7. The calibrated truck was believed to deliver a similar level of hazard to the bridges as that from the semi-rigid trailer, which caused the Skagit River bridge to collapse. Figure 10 shows the comparison of the collapse

mode of the bridge from the accident and simulations. A more detailed explanation of the collapse mechanisms can be found in Cao et al. (2020a).

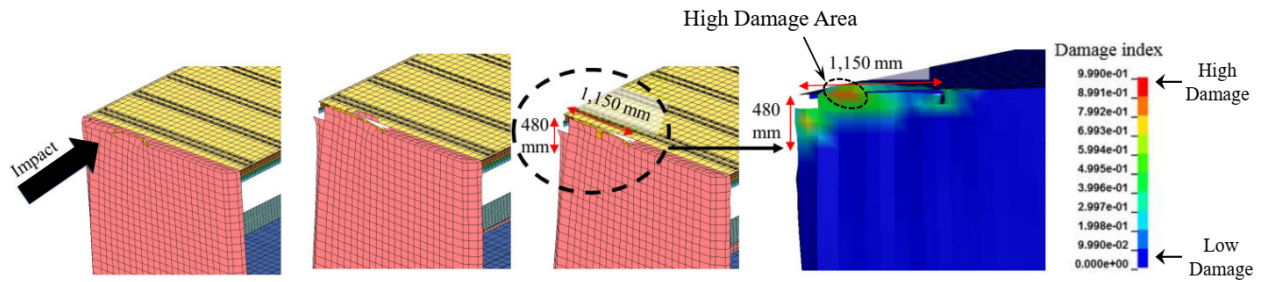


(a) Overall view of the simulation setup.

(b) Close-up of the impact location.

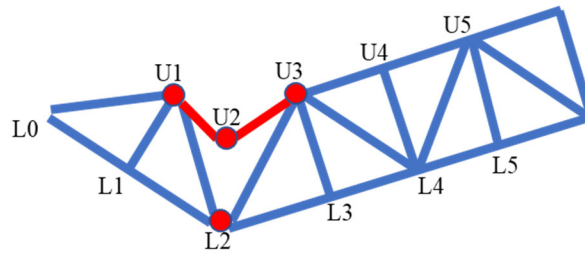
Source: FHWA

Figure 8. Photo. Simulation setup of overhead impact with Skagit River bridge in LS-DYNA.



Source: FHWA

Figure 9. Photo. Progress of the impact and damage mode of the trailer after impact.



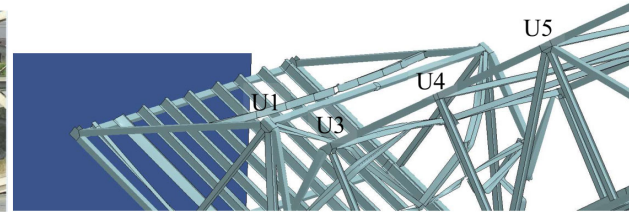
Source: FHWA

(a) Collapse mode simulated in LS-DYNA.



Source: NTSB

(b) Damaged truss structure after the actual accident.



Source: FHWA

(c) Damaged truss based on LS-DYNA simulation.

Figure 10. Photo. Comparison of the collapse scenario between the accident and FE simulation in LS-DYNA.

HAZARD LEVEL COMPARISON

To further compare the hazard level represented by the calibrated semi-rigid trailer and the original trailer model, a full-scale prestressed concrete girder bridge model was developed in LS-DYNA (Hallquist 2006). Figure 11 shows the simulation setup of the concrete girder subject to the overheight impact from the semi-rigid trailer model. The weight of the truck was assumed to be 80 kips and the velocity of the truck was 55 mph. The bridge model was developed based on the as-built drawing of a highway bridge in TX that had been subjected to several overheight impacts. More details about this bridge will be presented in the next chapter.

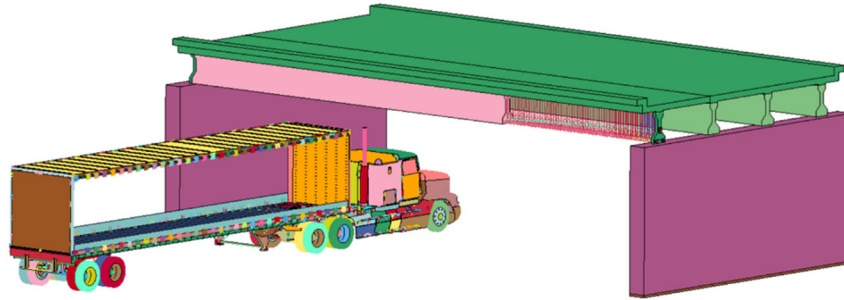
Material Model

Concrete behavior was modeled by the Continuous Surface Cap Model (CSCM MAT159) in LS-DYNA (Hallquist 2006). The model can capture key aspects of inelastic concrete behavior, including post-peak softening and confinement effects. It is based on an elasto-plastic damage formulation that accounts for rate effects. Default material parameters were used in this study, which were generated based on the compressive strength and the maximum aggregate size of the concrete (Murray et al. 2007). Steel rebars were modeled using Hughes-Liu beam elements and were represented using material Mat 3, which accounts for yielding and kinematic hardening plasticity. Steel rebar elements were assumed to fracture and removed after the strain reached 0.20. The general mesh size used was 1.5 inch. Perfect bond was enforced between the steel and concrete components by using the coupling method in LS-DYNA, *CONSTRAINED_BEAM_IN_SOLID.

The tendons in the bridge girder were unbonded. In the FE simulation, the *CONSTRAINED_BEAM_IN_SOLID command was used to model the tendons and their interaction with the surrounding concrete. The selected model ensures kinematic coupling (in displacement, velocity, and acceleration) between the tendons and concrete only in the direction normal to the tendon's axis but permits slip along the tendon's axis. Prestressing was achieved by cooling the tendons, which applied a prestressing force because of shrinkage in pre-stressing tendons. A similar approach has been used in many studies with reasonable simulation results (Nakalswamy 2010, Jiang and Chorzepa 2015, Do et al. 2018, Cao et al. 2019d). The pre-stressing tendons were modeled using ELASTIC_PLASTIC_THERMAL material (Mat 4), which can simulate the thermal deformations of the material based on provided temperature time history curves and a given coefficient of thermal expansion.

Validation

The concrete (Mat 159) and rebar (Mat 3) models have been validated for simulating the flexure/shear behavior of reinforced concrete (RC) specimens in multiple publications, including Moutoussamy et al. (2011), Liu (2012), and Murray et al. (2007). In these studies, multiple sets of experimental data of reinforced concrete (RC) beams subject to static or impact loading were used to prove the effectiveness of the RC modeling scheme. It has been shown that the selected modeling scheme yielded reasonable comparisons to the test results. The authors have used the same general modeling scheme described above in several previous studies where they conducted their own validation studies (Cao et al. 2019a, b, c, 2020b and Xu et al. 2019). The validation efforts in those research studies, which are not repeated here in the interest of saving space, provide confidence in the authors' nonlinear modeling approach.



Source: FHWA

Figure 11. Photo. Example concrete bridge model subject to the modified semi-rigid trailer impact.

Simulation Results

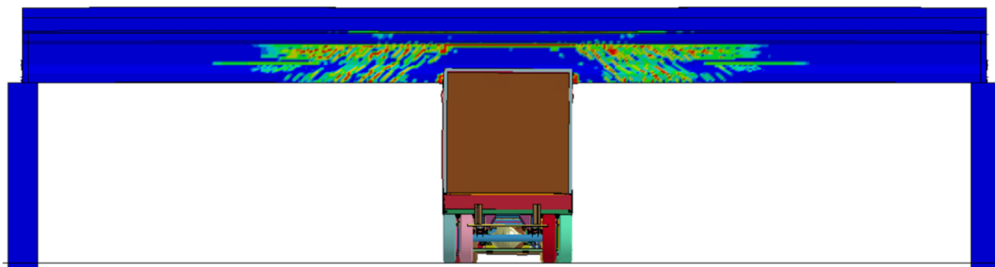
Figure 12 shows the simulated damage mode of the concrete girder subject to semi-rigid trailer impact and its comparison with damages to concrete girders because of overheight impacts. It can be seen from figure 12 that the simulation results well captured the typical trapezoidal shape yielding line patterns observed in many overheight impact accidents. Figure 13 shows the damage mode of the bridge girders subject to normal (soft) trailer impact. In figure 13, the top of the trailer was crushed and only some minor spalling was found in concrete girders. Such scratch type damage mode was also observed in some accidents shown in figure 13 when the colliding cargo was believed to be either soft or light in weight.

The objective of this study is to develop a demand model for designing a protection beam against severe overheight impacts. Therefore, the calibrated semi-rigid trailer model was used in parametric studies to achieve this objective.



Source: TxDOT

(a) Actual concrete girder damage mode.



Source: FHWA

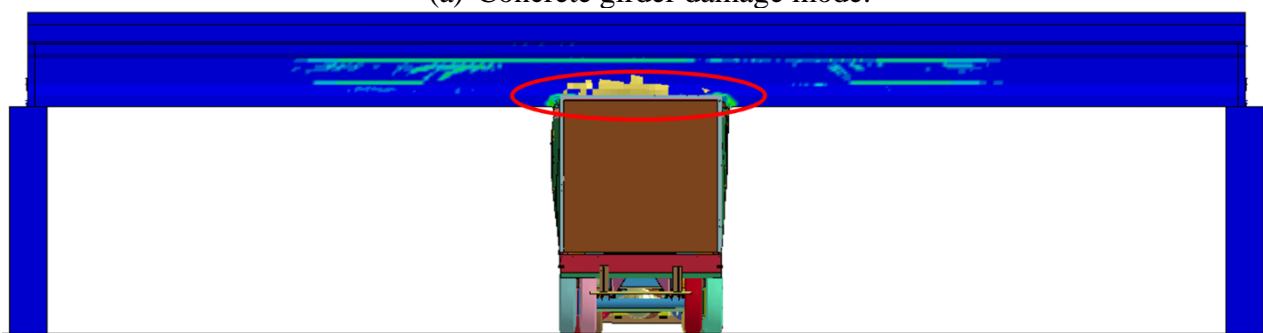
(b) Simulated girder damage mode in LS-DYNA.

Figure 12. Photo. Typical severe damage mode of the concrete girder subject to semi-rigid trailer impact.



Source: ODOT

(a) Concrete girder damage mode.



Source: FHWA

(b) Simulated girder damage mode.

Figure 13. Photo. Typical minor damage mode of the concrete girder subject to normal trailer impact.

PARAMETRIC STUDIES

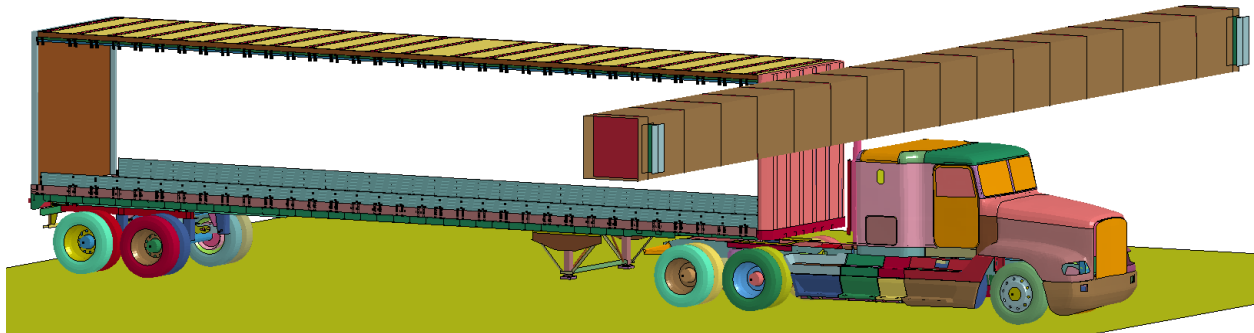
Figure 14 shows the setup of the prototype impact beam subjected to the semi-rigid trailer impact. The impact beam prototype was a steel box beam with a dimension of 40-inch x 40-inch x 2 inch. The size of the beam was consistent with the depth of the example prestressed concrete girder shown in figure 11 so that it could be aligned with the protected girder after installation. The span of the beam was around 66 ft (which is also the same as that of the example girder in figure 11). The steel beam was modeled using shell elements and was represented by material model Mat 3, which is the same as that for rebars in the concrete girders. The yield strength of the steel was 60 ksi.

To develop the demand model during an overheight impact, three different truck velocities were considered: 40 mph, 55 mph, and 70 mph, and three different truck weights were considered: 20 US ton, 30 US ton, and 40 US ton. In the following discussion, the name for each simulation case is described in the format of V-W, where V is the impact velocity (mph), W is the truck weight (US ton).

Figure 15 shows the impact responses of the steel beam for different truck velocities. In figure 15a, the peak impact force increased from 1,250 kips to 2,100 kips as the velocity was increased from

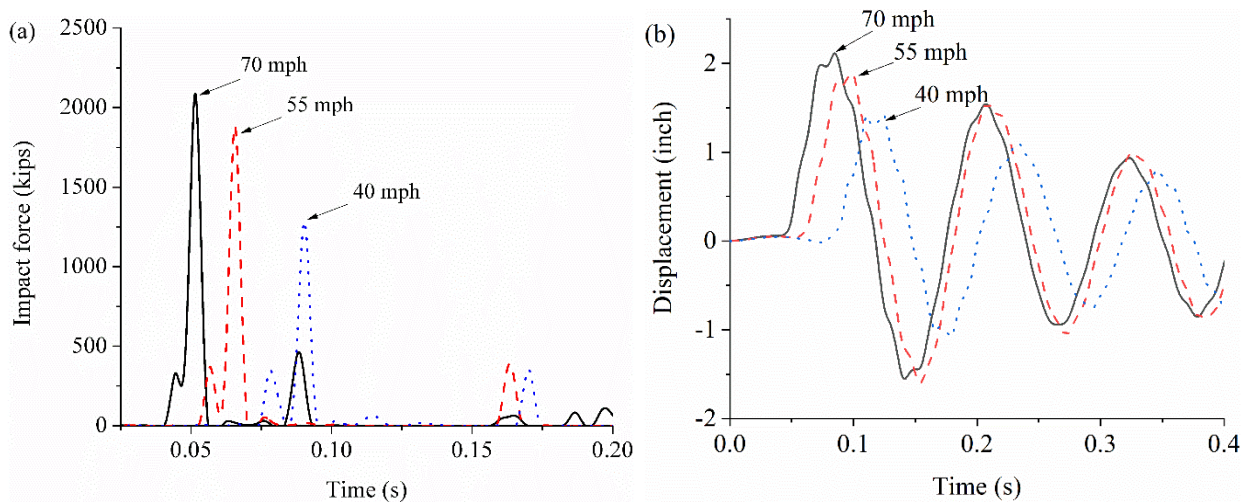
40 mph to 70 mph for a 20-ton truck. Figure 15b shows the displacement time histories of the impact beam subject to the trailer impact, in which the peak deformation of the beam increased from 1.5 inch to 2.1 inch as the velocity of the truck was increased from 40 mph to 70 mph.

Figure 16 shows the impact responses of the steel beam for different truck weights, where the truck speed is 70 mph. In figure 16a, the peak impact force increased from 2,100 to 3,050 kips as the truck weight was increased from 20 ton to 40 ton. The deformations of the beam were shown in figure 16b, where the peak deformation increased from 2 inch to 8 inch as the weight of the truck was increased from 20 ton to 40 ton.



Source: FHWA

Figure 14. Photo. Simulation setup of overheight impact with steel box beam.

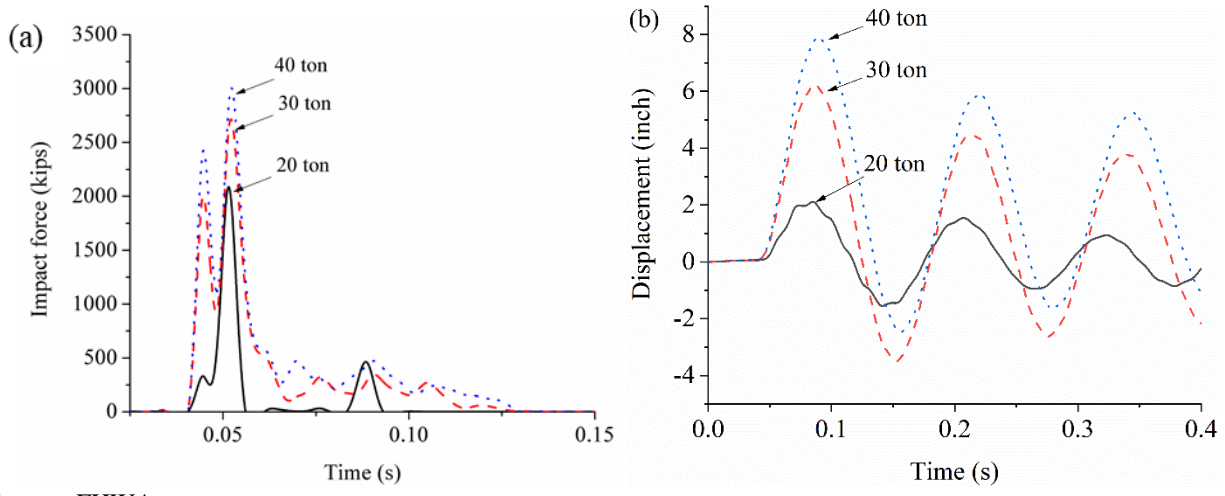


Source: FHWA

(a) Impact force time histories.

(b) Displacement time histories.

Figure 15. Graph. Impact responses for steel beams with truck weight of 20 tons.



Source: FHWA

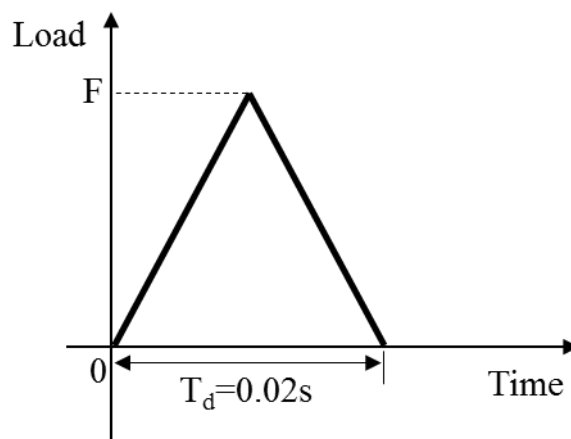
(a) Impact force time histories.

(b) Displacement time history.

Figure 16. Graph. Impact responses for steel beams with truck speed of V70.

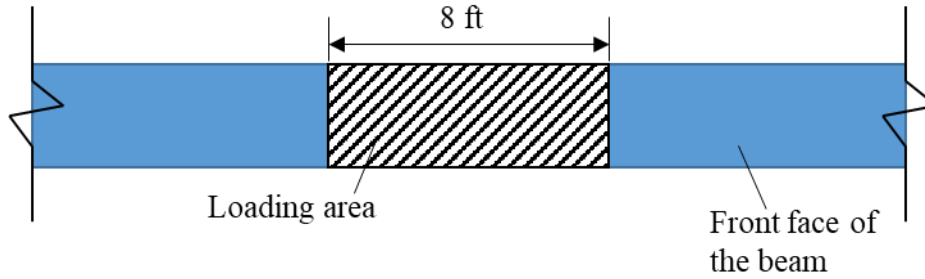
SIMPLIFIED PULSE MODEL FOR OVERHEIGHT IMPACT

Based on the analysis of the impact force time histories for various truck weight/velocity combinations, a simplified triangular pulse is proposed and is shown in figure 17 to represent the demand model of overheight impact from semi-rigid trailers. Based on the observations from parametric simulation cases with a truck velocity varying from 40 mph to 70 mph and truck weight varying from 20 ton to 40 ton, the duration of the pulse was assumed to be 0.02 sec and the peak loading, F, was dependent on the truck velocities and weight. Figure 18 illustrates the loading scheme for the proposed pulse model, where the pulse was applied as a distributed force on the impact beam over a length of 8 ft, representing the width of the standard trailer used in this study.



Source: FHWA

Figure 17. Graph. Simplified triangle pulse loading model.



Source: FHWA

Figure 18. Illustration. Loading application of the pulse model.

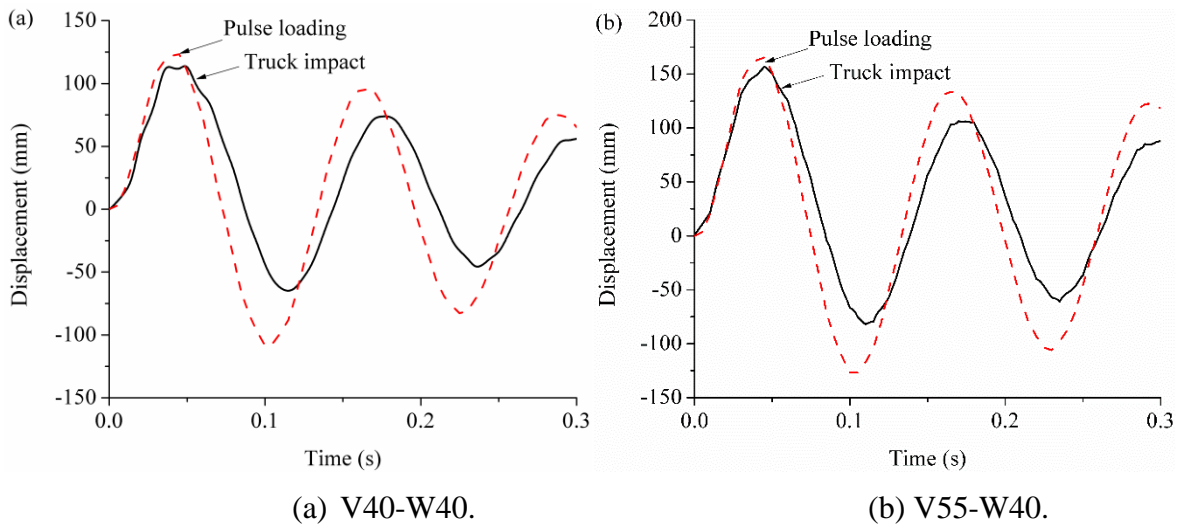
The peak force of the proposed pulse model was calibrated so that the pulse model causes the same displacement of the beam as that from truck impact. Based on a systematic parametric study, where all key parameters have been varied, a general equation for the peak impact, similar to that in AASHTO (2017) for vessel collisions, can be obtained through nonlinear regression of simulation results as,

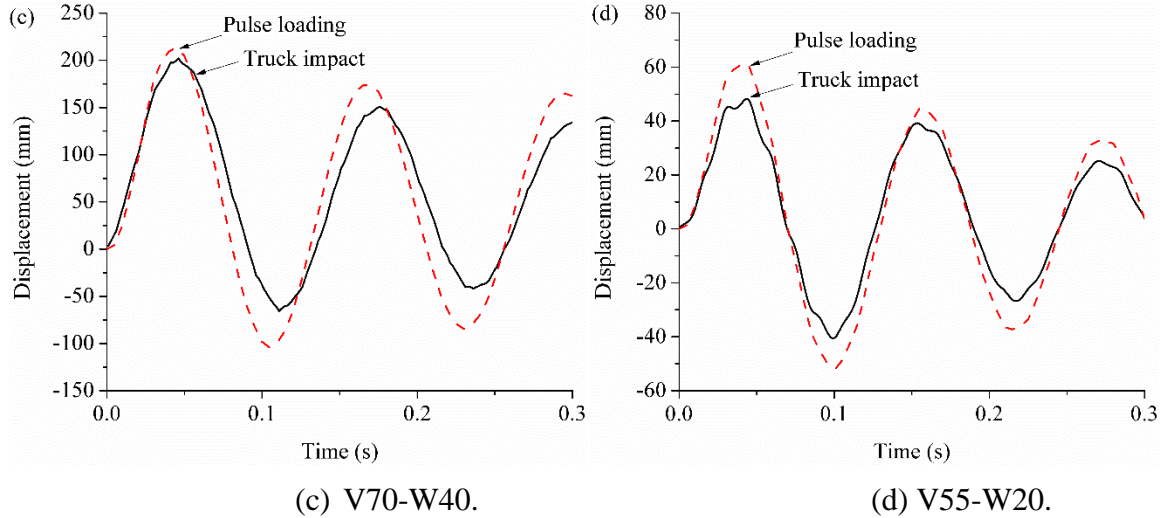
$$F = 0.75V^{0.84}W^{1.35} \quad (1)$$

where, F is the peak force (kips), V is the truck impact velocity (mph), W is the truck weight (US ton).

It should be noted that the form of the demand model in equation (1) is similar to that for the impact of trucks on bridge piers defined in Agrawal et al. (2018), Cao et al. (2019b), and Xu et al. (2019).

Figure 19 shows the comparison of the beam displacement from the truck and pulse simulations. It can be seen from figure 19 that the pulse simulation results match the truck simulation results reasonably well. Table 1 lists the results of the calibrated pulse force from the FE simulations and that from the proposed demand model based on equation (1).





Source: FHWA

Figure 19. Graph. Comparison of the beam displacement caused by the truck impact and pulse loading.

It should be noted that the peak force from equation (1) is impulsive in nature and has a relatively short duration. As such, direct use of the estimated dynamic load in the traditional static design framework may lead to overconservative results. Instead, the dynamic load from equation (1) for a particular impact velocity and truck weight could be used in a performance-based framework in the next section to directly obtain the required capacity to satisfy a certain performance level.

Table 1. Comparison of calibrated pulse demands in Finite Element Model (FEM) and proposed equation results

Simulation	FEM (kips)	Equation 1 (kips)	Equation 1/FEM
V40-W40	2305.35	2418.65	1.05
V55-W40	3040.01	3160.44	1.04
V70-W40	3749.21	3870.12	1.03
V40-W30	1922.04	1640.23	0.85
V55-W30	2573.89	2143.28	0.83
V70-W30	3080.70	2624.56	0.85
V40-W20	765.83	948.82	1.24
V55-W20	1053.77	1239.81	1.18
V70-W20	1162.71	1518.22	1.31
Average			1.04

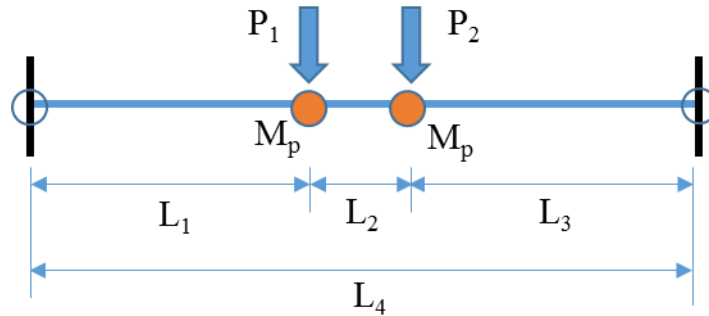
PERFORMANCE-BASED DESIGN

A performance-based design framework requires determination of three things: 1) demand (D), 2) capacity (C), and 3) a performance objective for a given hazard level. In general, the computation of demand for the vehicular impact problem is complicated because it entails running a full vehicle model. However, that can be greatly simplified by using the proposed demand equation and

exploiting the previously discussed observation that the force time histories have similar characteristics and loading effects on the impact beams.

The proposed performance-based design method correlates the ductility of the girder with the demand to capacity (D/C) ratio, where D is the dynamic impact force from equation (1) and C is the plastic capacity of the steel beam, as illustrated in figure 20 and equation 2. The proposed approach has conceptual similarities to a method proposed by the authors for the design of bridge piers impacted by both single unit (SU) and TS trucks (Agrawal et al. 2018 and Cao et al. 2019b).

In the design of structures against vehicular impact, the performance objective is typically a qualitative one, e.g., minor or major damage, as defined in Liu (2012). In this study, the performance was quantified using the ductility ratio of the impact beam, which is the maximum deformations over the yielding deformation. The yielding deformation was determined based on the pushover simulation, where an 8-ft distributed pushover load was applied in the middle of the impacted beam (similar to the loading application in figure 18). Impact beams with minor damage, i.e., ductility ratio less than 1.0, are fully functional after the impact and do not need immediate attention. Yielding damage is associated with the ductility ratio larger than 1.0 with permanent damage in the beams and may need temporary closure of the road for immediate repair or replacement after the impact event. A steel beam with yielding damages will not collapse and the impacting trailer will be stopped or effectively deformed so that it would not impact the protected concrete girders.



Source: FHWA

Figure 20. Graph. Capacity calculation model for steel box beams.

$$C = P_1 + P_2 = \frac{M_p}{L_1} + \frac{M_p}{L_3} = M_p \left(\frac{1}{L_1} + \frac{1}{L_3} \right) \quad (2)$$

where,

L_2 = width of the trailer, 8 ft.

$L_1 = L_3 = 0.5 \times (L_4 - L_2)$.

L_4 = span length of the beam.

M_p = plastic moment of the steel beam.

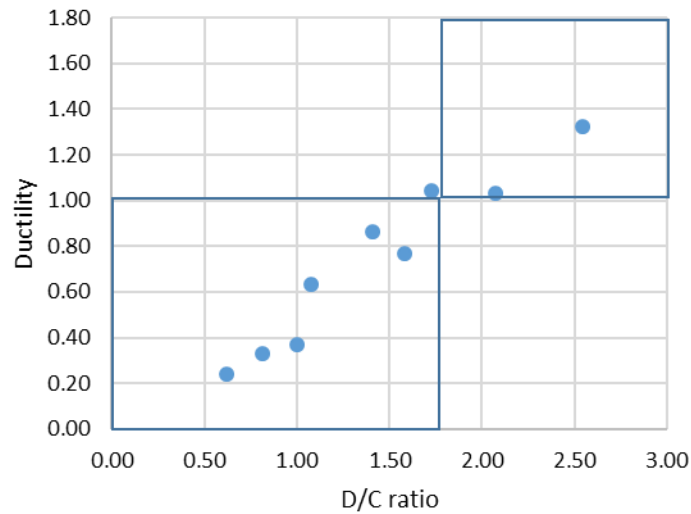
C = lateral capacity of the beam.

Table 2 lists the ductility ratios calculated for each truck-impact beam simulation. Figure 21 shows the plot of the ductility of the impacted beam as a function of the D/C ratio for the nine cases of semi-rigid trailer impact on the barrier. It is observed from figure 21 that two levels of

performance, i.e., minor and yielding damage, can be clearly distinguished in terms of the D/C ratio.

Table 2. Computed ductility ratio for the impact beams subject to truck impact

Simulation	Ductility	Damage level
V40-W20	0.24	Minor
V55-W20	0.33	Minor
V70-W20	0.37	Minor
V40-W30	0.63	Minor
V55-W30	0.86	Minor
V70-W30	1.04	Yielding
V40-W40	0.77	Minor
V55-W40	1.03	Yielding
V70-W40	1.33	Yielding



Source: FHWA

Figure 21. Graph. Performance based design chart for the steel box beam.

The performance levels in terms of ductility and D/C ratios are listed in table 3 below. The information presented in table 3 can be used to design an impact beam to achieve the desired performance level as discussed in the next section.

Table 3. Performance levels, corresponding damage state, and rotation.

Performance level	Damage state	D/C	Ductility
Immediate use	Minor damage	[0.00, 1.75]	[0.0, 1.0]
Need repair/ replacement	Yielding damage but stopped the trailer	[1.75, 2.75]	[1.0, 1.8]

PROPOSED DESIGN PROCEDURE

The information from figure 21 and table 3 can be used to establish a performance-based design methodology that applies to impact beam designs. The proposed design steps are as follows:

1. Select the speed and weight of the impacting tractor-semitrailer based on local traffic conditions and owner requirements.
2. Determine the desired performance level: Immediate use (minor damage) or Need repair/replacement (yielding damage). Select from the ranges in table 3 an acceptable D/C ratio.
3. Compute the demand, D , using design equation (1) for the selected truck speed, weight through dynamic analysis using any commercial structural analysis software.
4. Determine the required capacity of the beam, $C = D/(\text{selected } D/C \text{ ratio})$.
5. Select the section size and steel strength to satisfy C . Compute the actual capacity of the beam, C_{design} , using the plastic capacity analysis shown in equation (2).

VALIDATION OF THE PROPOSED FRAMEWORK

Three impact beams with characteristics that are different than those used during the calibration of the demand model were selected to validate the proposed performance-based design framework. The geometries and strengths of the selected beams are shown in table 4. The steel beams were designed according to the procedure detailed above. These steel beams were then impacted by the calibrated tractor-semitrailer with different combinations of weight and approach speeds, as outlined in table 5, creating a total of 7 cases that cover a broad range of design scenarios. A unique descriptive name is given to each case of simulation in table 4. For example, V-W, where V is the impact velocity (mph), W is the truck weight (US ton). The actual deformation and ductility ratios were computed for each case. These values are listed in table 5 along with the computed damage states according to the criteria in table 3. As shown in table 5, the predictions are accurate for all the cases. This shows that the proposed framework is reasonable and can be used to achieve the desired performance level for a bridge at a risk of being impacted by a truck, given the complexity of the collision process being modeled.

Table 4. Beam geometry for validation study

Beam ID	Beam section dimension (inch)	Beam section thickness (inch)	Beam span (ft)	Steel strength (ksi)	C_{design} (kips)
1	40	2.0	32	60	3543
2	30	1.5	32	60	1495
3	40	2.0	48	60	2113

Table 5. Selected cases for validation of proposed method

Case	Truck characteristics	Beam ID	D/C	Predicted damage level	Ductility	Actual damage level
1	V55-W20	1	0.53	Minor	0.38	Minor
2	V55-W30	1	0.76	Minor	0.91	Minor
3	V40-W40	2	1.63	Minor	0.77	Minor
4	V55-W40	2	2.14	Yield	1.11	Yield
5	V70-W40	2	2.62	Yield	1.69	Yield
6	V60-W30	3	1.10	Minor	0.88	Minor
7	V50-W30	3	0.95	Minor	0.80	Minor

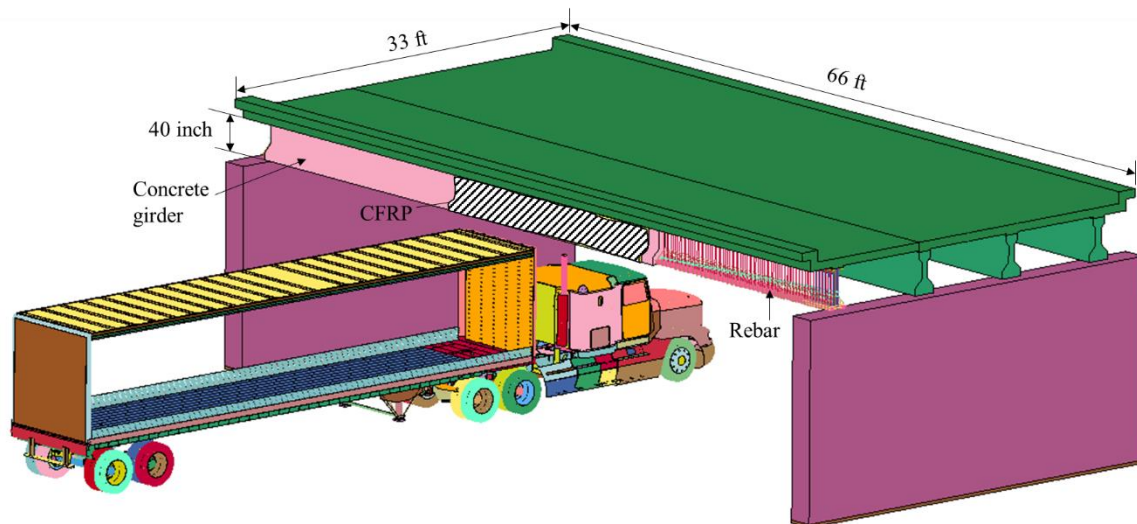
CHAPTER 3. RETROFIT OF GIRDERS DAMAGE DURING OVERHEIGHT IMPACT USING CARBON-FIBER REINFORCED POLYMERS

Composites such as carbon fiber-reinforced polymers (CFRP) have been widely used to increase the ultimate strength of reinforced concrete (RC) and pre-stressed concrete members through externally bonded FRP systems (Belarbi et al. 2012; Rosenboom et al. 2009). More recently, the use of composite materials in the strengthening, rehabilitation, and repair industry has been gaining popularity due to their excellent material behavior and ease of application. However, the effectiveness of CFRP in protecting pre-stressed girders impacted by overheight vehicles is not well established because of the lack of guidance on the application of CFRP and evaluation of its effectiveness. Hence, the proposed research used high-fidelity simulations to investigate the behavior of several pre-stressed concrete girders wrapped by CFRP when impacted by overheight vehicles.

MODEL OF THE TRUCK AND BRIDGE

Bridge Model

Figure 22 shows the full-scale prestressed concrete girder bridge model developed in LS-DYNA (Hallquist 2006). The bridge model was developed based on the as-built drawing of a highway bridge in Texas that has been subjected to several overheight impact accidents (Figure 23). Figure 24 shows the application of CFRP wrap on the example bridge girders. In figure 24, the total length of the CFRP was around 1/3 of the total span of the bridge, which is close to the width of the roadway underneath the girder. The CFRP wrapping was applied from the bottom of the girder to the web of the girder.



Source: FHWA

Figure 22. Photo. Example concrete bridge model subject to the modified semi-rigid trailer impact.

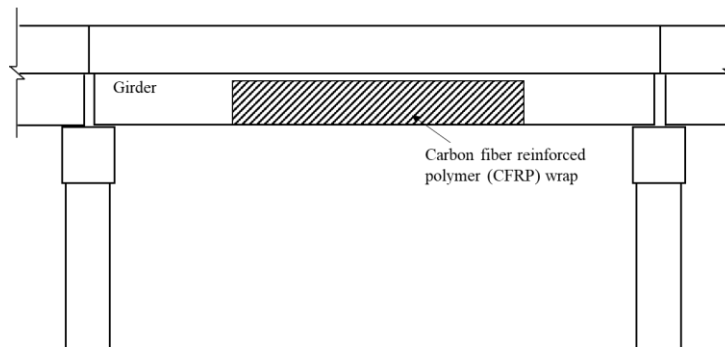


Source: TxDOT

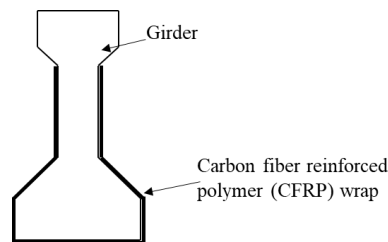
(a) Before the impact.

(b) Post-impact scene.

Figure 23. Photo. Example prestressed concrete bridge.



(a) Location of CFRP wrapping on the concrete girder.



(b) Cross section of the girder with CFRP wrapping.

Source: FHWA

Figure 24. Illustration. Illustration of CFRP wrapping on prestressed concrete girders.

Material Model

As shown in figure 22, the concrete behavior was modeled by the Continuous Surface Cap Model (CSCM MAT159) in LS-DYNA (Hallquist 2006). Steel rebars were modeled using Hughes-Liu beam elements with material model Mat 3, which accounts for yielding and kinematic hardening plasticity. Steel rebar elements were assumed to fracture and removed after the strain reached 0.20. More details about the material models and validations for the concrete, steel rebars, and tendons can be found in Chapter 2.

The CFRP sheet was modeled using ENHANCED_COMPOSITE_DAMAGE (MAT55) in LS-DYNA (Hallquist 2006). The material was defined as elastic before reaching its failure strain and

elements would be deleted (fracture) after reaching the maximum allowable strain. The young's modulus of the CFRP was 32,915 ksi and the failure strain was around 0.0167 based on the manufacture information provided by TxDOT. Shell elements were used to model the CFRP wrapping, which were fully merged with the concrete girders. The failure mode of debonding was not modeled in this study. The thickness of the CFRP wrapping was 0.08 inch based on the manufacture's information.

SIMULATION RESULTS

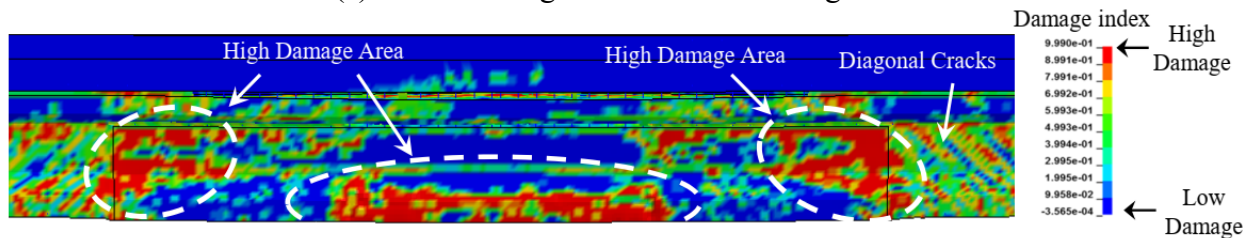
Based on the setup in figure 22, numerical simulations were carried out to identify the typical damage mode of CFRP wrapped concrete girders subject to overweight truck impact. In the simulation, the velocity of the truck was 55 mph and the weight of the truck was 40 US ton. Based on the simulation, figure 25 shows the comparison of the simulated damage mode of the girder and the actual damaged girder during the overweight impact accident in figure 23. It can be seen from figure 25 that diagonal cracking was developed in the front face of the girder's web. Most of these inclined cracks were developed outside the wrapping area. Also, horizontal yield lines were developed between the web and top/bottom flanges, which indicated the typical weak locations of I-girders in the lateral direction.

Figure 26 shows some localized damage of the CFRP sheet (fracture) caused by the edge of the impinging semi-rigid trailer. In figure 25, similar patterns of CFRP fracture were also observed in the bottom flange of the damaged girder.



Source: TxDOT

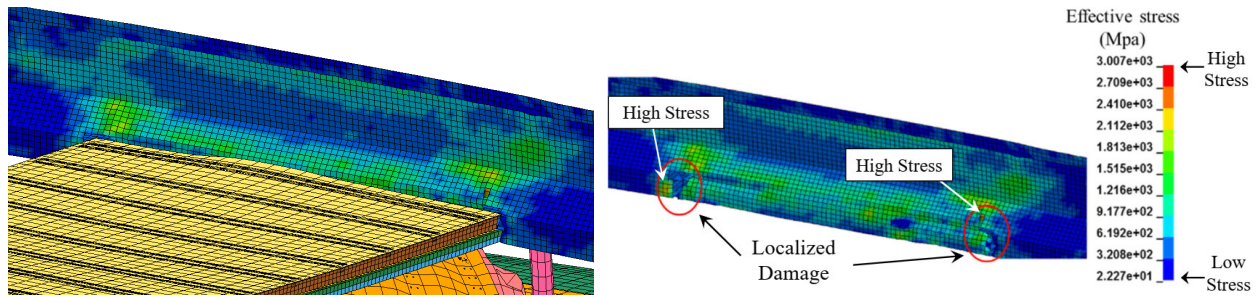
(a) Actual damage mode of the CFRP girder.



Source: FHWA

(b) Simulated damage mode of the CFRP girder.

Figure 25. Photo. Typical damage mode of the CFRP wrapped girders subject to overweight impact from actual accidents and simulations.



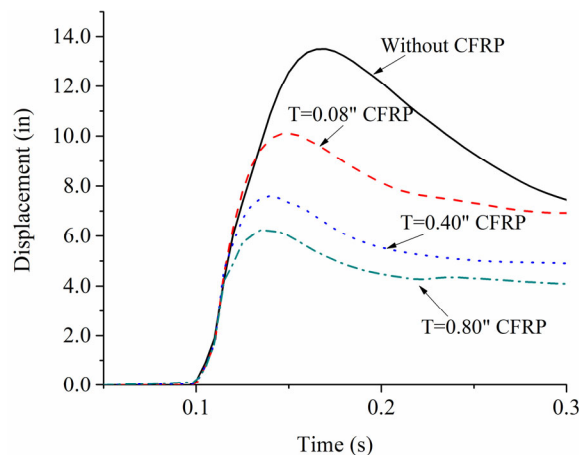
Source: FHWA

(a) Trailer impact with the CFRP girder. (b) Damage mode of the CFRP by trailer impact.

Figure 26. Photo. Localized damage of the CFRP wrapping from the simulation.

PARAMETRIC STUDY

Figure 27 shows the effects of CFRP thickness on the deformation of concrete girders, where the velocity and weight were the same as the example above, i.e., 55 mph and 40 US ton. In figure 27, the peak deformation of the girder without CFRP wrapping was 13.8 inches and the permanent deformation was around 7 inches. After applying the 0.08-inch thick CFRP, the peak deformation was reduced from 13.8 inch to 11 inches, while the permanent deformation of the CFRP girder was similar to the results without CFRP wrapping. To investigate the effect of CFRP thickness on the girder deformations, the thickness of CFRP sheet was changed from 0.08 inch to 0.80 inch. In figure 27, the peak deformation of the girder decreased from 11 inches to 6.2 inches (44% less) as the thickness was increased from 0.08 inch to 0.80 inch, which shows certain confinement effects from the thick CFPR sheets. However, the permanent deformation was still large for the 0.80-inch CFRP wrapping case and was only reduced by 36% as the thickness was increased by 10 times, and the concrete girder was found significantly damaged, showing a damage mode similar to that in figure 25.



Source: FHWA

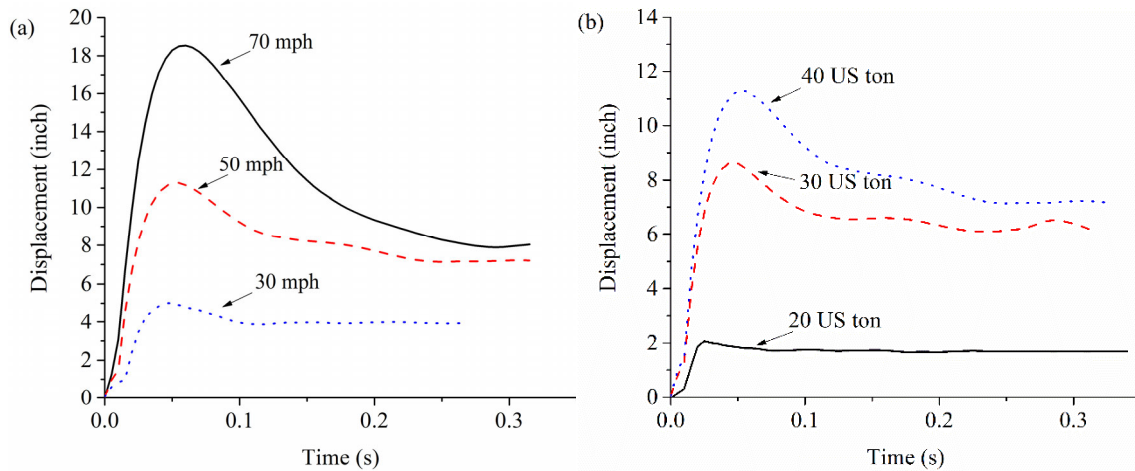
Figure 27. Graph. Effects of CFRP on the girder deformations subject to overheight impact (V55-W40).

Figure 28 shows the deformation of the 0.08-inch thick CFRP wrapped girder subjected to different truck velocities and truck weights. In figure 28a, the permanent deformation of the girder increased from 4 inch to 9 inch as the velocity of the truck was increased from 30 mph to 70 mph. Also, in

figure 28b, the girders' permanent deformation increased from 2 inch to 8 inch as the weight of the truck was increased from 20 US ton to 40 US ton for a truck speed of 50 mph.

Figure 29 shows the impact force time histories for a 40-ton truck impacting the CFRP girder at different velocities. In figure 29, the impact force shows impulsive nature and the peak impact force increased from 1,350 kips to 1,978 kips as the velocity was increased from 30 mph to 50 mph. The peak impact force was found to be decreased from 1,978 kips to 1,619 kips as the velocity was increased from 50 mph to 70 mph. This is because the girder was more severely damaged by the 70-mph truck than that by the 50-mph truck.

Figure 30 shows the damage mode of the CFRP wrapped girder subject to an overweight truck at different speeds. The simulation results show that the CFRP wrapped girder doesn't have sufficient capacity to resist the impact load from the overweight truck.

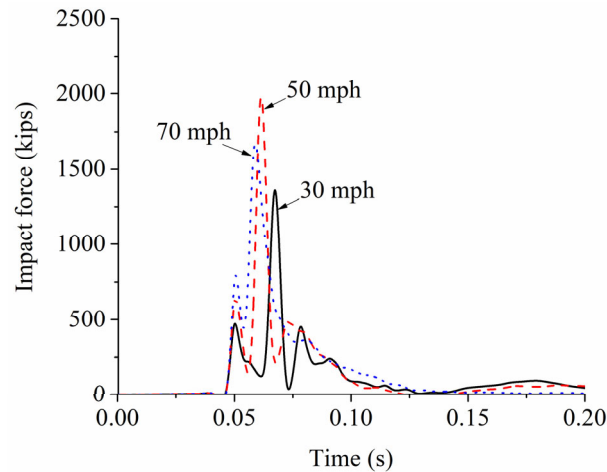


Source: FHWA

(a) Effect of different speeds.

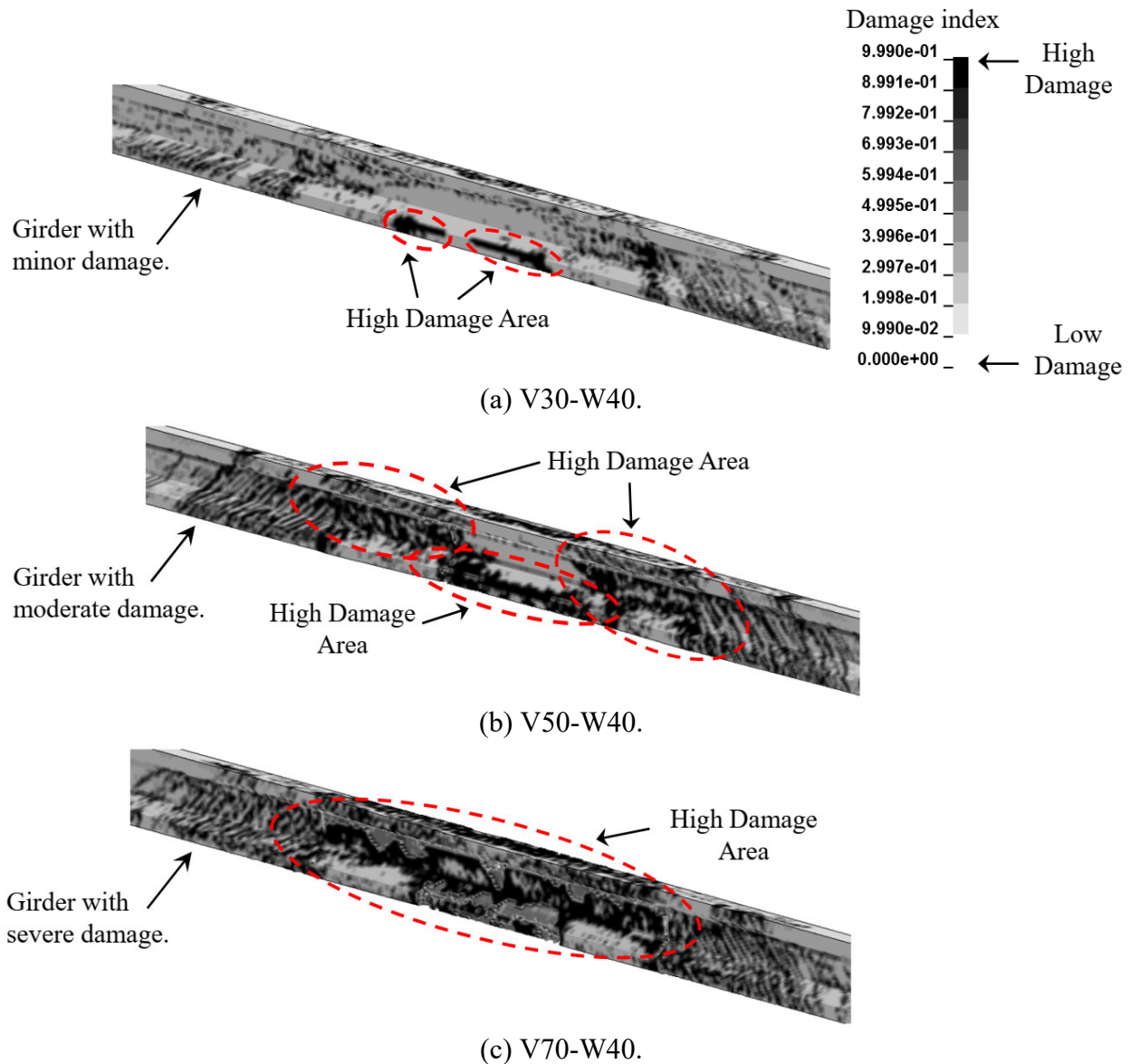
(b) Effect of different truck weights.

Figure 28. Graph. Deformation of the CFRP wrapped girder subject to different truck impact.



Source: FHWA

Figure 29. Graph. Impact force time history for a 40-ton truck at different speeds.

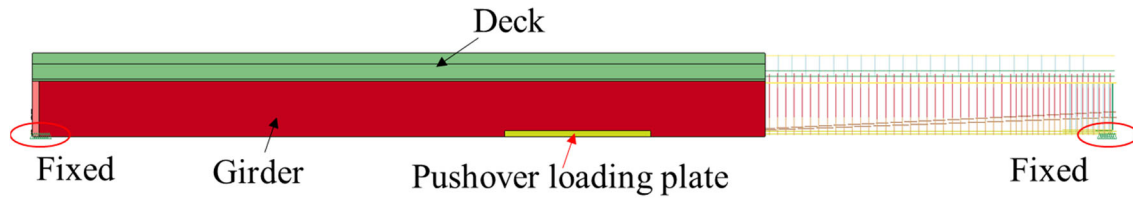


Source: FHWA

Figure 30. Photo. Damage mode of the CFRP wrapped girder.

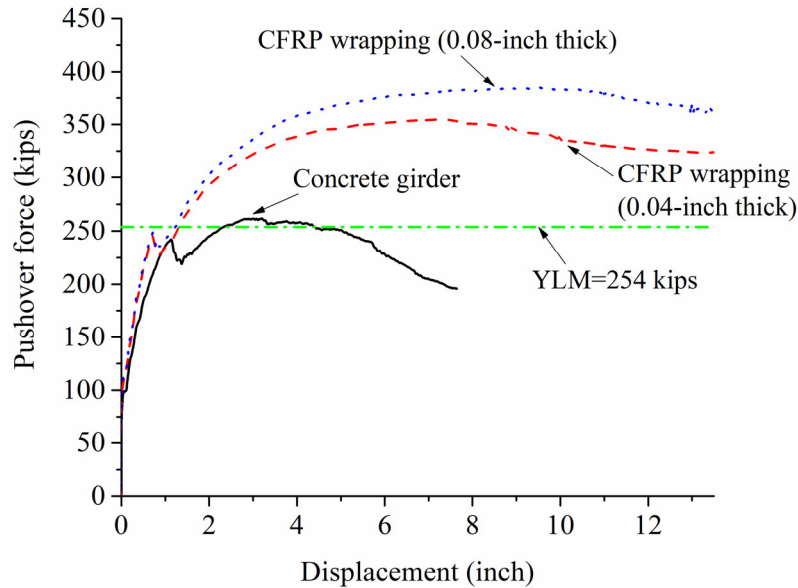
PUSHOVER ANALYSIS SIMULATION

The simulation results shown in figure 25 and figure 27 indicated that CFRP wrapping was not effective in preventing severe damage or large deformations of concrete girders under the overheight impact. To better study the lateral capacity enhancement by the CFRP wrapping, pushover simulations were conducted on the concrete girders with and without CFRP. Figure 31 shows the setup of the pushover loading in LS-DYNA, where the loading length was around 8 ft representing the width of the trailer. Based on the simulation, figure 32 shows the load-deflection curves for the concrete girder with and without CFRP. It can be seen from figure 32 that the peak loading of the girder was increased from 261 kips to 354 kips (0.04-inch thick CFRP) and 384 kips for 0.08-inch thick CFRP, which is still much less than the peak dynamic loading from the truck impact shown in figure 29, even for a low-speed impact of 30 mph.



Source: FHWA

Figure 31. Illustration. Pushover loading setup on the concrete girder.

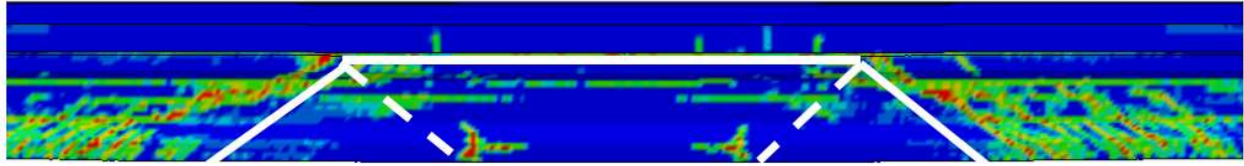


Source: FHWA

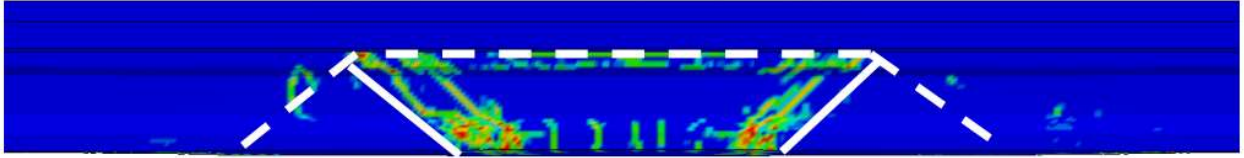
Figure 32. Graph. Pushover curve from the simulation.

Figure 33 shows the yield line patterns of the concrete girder obtained from the pushover simulations. In figure 33, several inclined yield lines have been seen to develop in the front face and back face of the girder. Also, a horizontal yield line occurred at the interface between the deck and the girder. The overall damage pattern appeared to be a W-shape based on the simulations. To estimate the lateral capacity of the concrete girder, figure 34 shows the yield line method calculations based on the W-shape damage patterns obtained from the simulations. Based on the energy balance method, equation (3) shows the calculation of the lateral capacity of the concrete girder using the yield line method.

Using equation (3), the calculated capacity of the concrete girder was around 254 kips, which matched the pushover simulation results reasonably well (Figure 32). It should be noted that similar W-shape yield line patterns have also been seen in concrete barriers subject to lateral loading and a similar yield line method was developed recently by Cao et al. (2020b) to predict the flexural strength of concrete barriers. Based on the comparison shown in figure 32, the lateral capacity of the concrete girder can be estimated by the proposed YLM, which can be used in designing other alternative protection devices, such as honeycombs. Details about the design process for alternative protective systems will be discussed next.



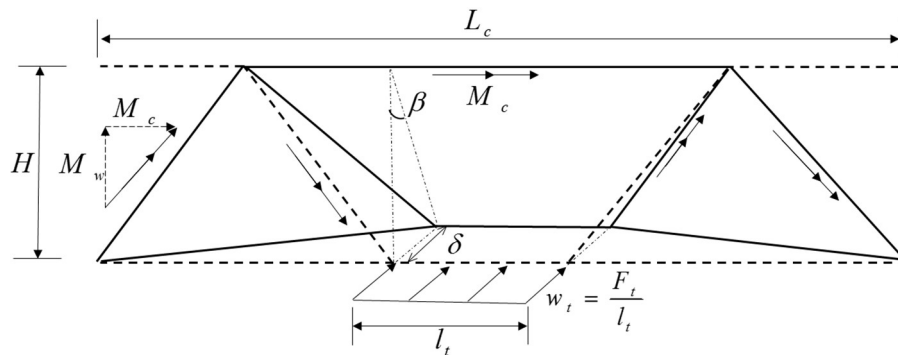
(a) Front face.



(b) Back face.

Source: FHWA

Figure 33. Graph. Patterns of the yield lines of concrete girder under pushover loading.



Source: FHWA

Figure 34. Illustration. Illustration of the yield line method.

$$C_{girder} = F_t = \frac{2M_w}{H} + 6M_c + \frac{M_c l_t}{H_l} \quad (3)$$

where:

C_{girder} = lateral capacity of the girder.

F_t = lateral force.

H = height of the girder.

l_t = longitudinal length of distribution of impact force F_t .

M_c = flexural resistance of the cantilevered wall (girder) about an axis parallel to the longitudinal axis of the bridge.

M_w = flexural resistance of the girder about its vertical axis.

CHAPTER 4. OVERHEIGHT IMPACT ON GIRDERS WITH HONEYCOMB LAYERS

Based on the studies shown above, the CFRP wrapping was found to be ineffective in protecting girders against overheight impact. The main reason is that CFRP wrapping did not sufficiently enhance the lateral capacity of the girder. On the other hand, it is well known that the ability of CFRP to absorb impact energy is rather limited. As an alternate protection strategy, this research investigated the effects of energy-dissipative honeycombs on the impact protection of concrete girders.

Energy Method for Honeycomb Device Design

To protect the girder from overheight impact, there are two criteria for the honeycomb design: 1) the crushing force should be lower than the girder's lateral capacity; 2) the honeycomb should be thick enough to dissipate enough energy from the impacting truck. Equations (4) and (5) show the calculation of the crushing force and energy dissipated by the honeycomb.

$$\sigma_{crush} A_{effective} < C_{girder} \quad (4)$$

$$E_{honeycomb} = \sigma_{crush} A_{effective} d \quad (5)$$

where σ_{crush} is the crushing strength; $A_{effective}$ is the effective contact or crushing area between the overheight cargo and the honeycomb, C_{girder} is the lateral capacity of the girder (estimated by equation 3); $E_{honeycomb}$ is the energy dissipated by the honeycomb block, and d is the thickness of the honeycomb in the impact direction.

Based on the yield line method proposed in equation (3), the lateral capacity of the girder (C_{girder}) was estimated to be 254 kips. Therefore, the designed crushing force should be lower than 254 kips to prevent severe damage to the girder under the impact load. Based on the simulation setup, the crushing area of the honeycomb ($A_{effective}$) was estimated to be 4,400 in². Therefore, the design crushing strength of the honeycomb should be lower than $C_{girder}/A_{effective} = 254\text{kips}/4,400\text{in}^2 = 58$ psi. In this study, the crushing strength was 29 psi for conservative design.

Based on the energy balance method, equations (6) and (7) show that the kinetic energy from the colliding truck should be equal to the deformation energy dissipated by the honeycomb and the truck itself under the condition that the truck is fully stopped, i.e.,

$$E_k = E_{honeycomb} + E_{truck} \quad (6)$$

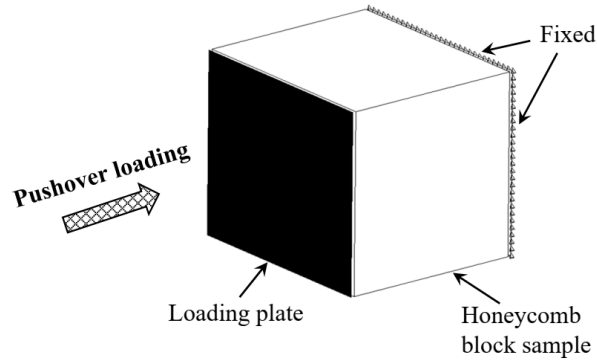
$$E_k = \frac{1}{2} MV^2 \quad (7)$$

where E_k is the kinetic energy from the truck and E_{truck} is the deformation energy by the truck itself due to the collision, M is the weight of the truck and V is the velocity of the truck.

Validation of the Honeycomb Modeling

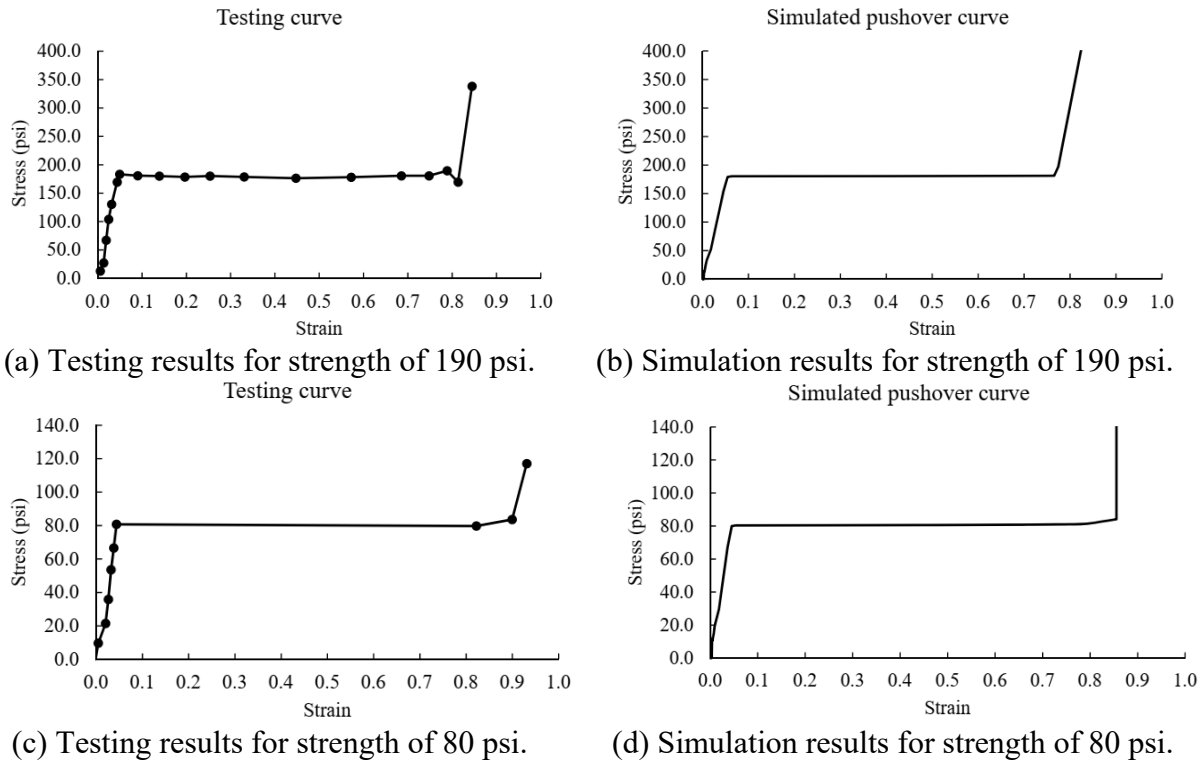
In this work, the honeycomb was modeled using solid element in LS-DYNA and the crushing behavior was simulated using MAT_HONEYCOMB (MAT26). To validate the material modeling, compression testing results from the honeycomb manufacture were used to compare

with the simulation data. Figure 35 shows the pushover simulation setup of the honeycomb block. Based on the setup in figure 35, the lateral loading was applied slowly, and the compressive stress-strain curve of the honeycomb was obtained from the simulations. Figure 36 shows the comparison of the testing results and the simulation data. Two different crushing strengths of the honeycomb were selected: 190 psi and 80 psi. It can be seen from figure 36 that the simulation results match the testing data reasonably well, especially for the crushing stage where most of the energy was dissipated.



Source: FHWA

Figure 35. Photo. Simulation setup of pushover on the honeycomb sample.



Source: FHWA

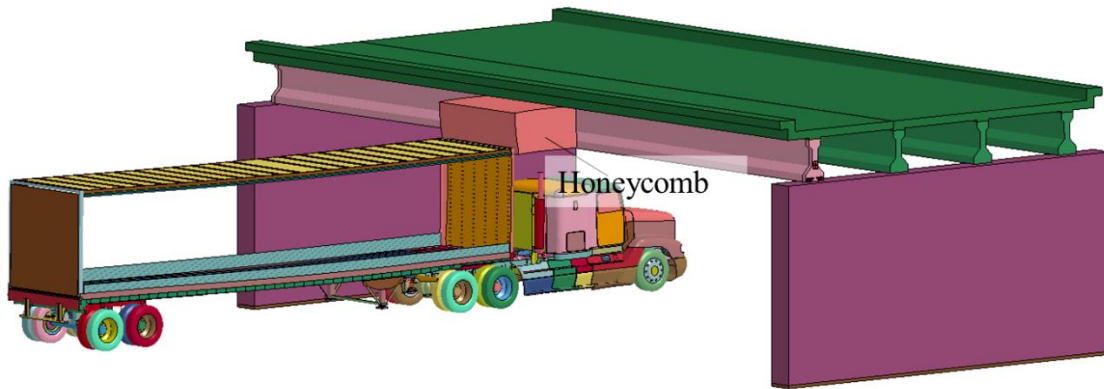
Figure 36. Graph. Pushover curves of the honeycomb.

Truck Impact Simulation

Figure 37 shows the simulation setup of the overweight impact with a honeycomb block installed on the fascia girder of the bridge. The truck and bridge models were the same as those used in the

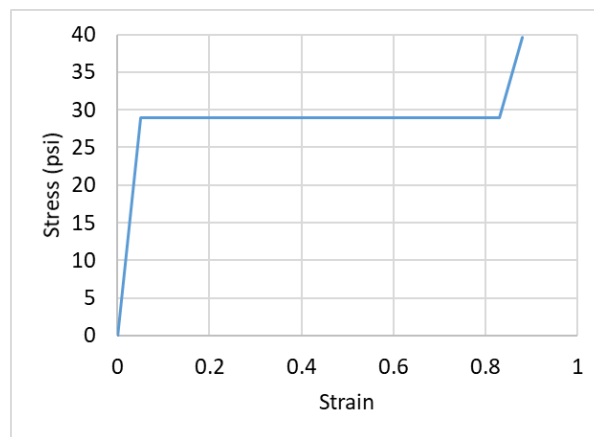
CFRP simulation studies. In this study, the length and depth of the honeycomb was 110-inch x 40 inch, which fit the width of the impacting trailer and the depth of the concrete girder. The thickness of the honeycomb was 80 inches, which was designed to stop the tractor-trailer at a high velocity, up to 113 kph, ensuring enough capacity for energy dissipation.

Figure 38 shows the stress-strain relationship of the honeycomb model in the simulation. The stress-strain curve was based on crush testing data from the product manufacture. In this study, the crushing strength was selected as 29 psi. In figure 38, the honeycomb will be completely compressed as 82% of the honeycomb volume was being crushed. The crushing stage of the honeycomb was defined from the beginning to the strain of 82%, where most of the energy was dissipated during this stage.



Source: FHWA

Figure 37. Photo. Simulation setup of honeycomb modular subject to the overheight impact.

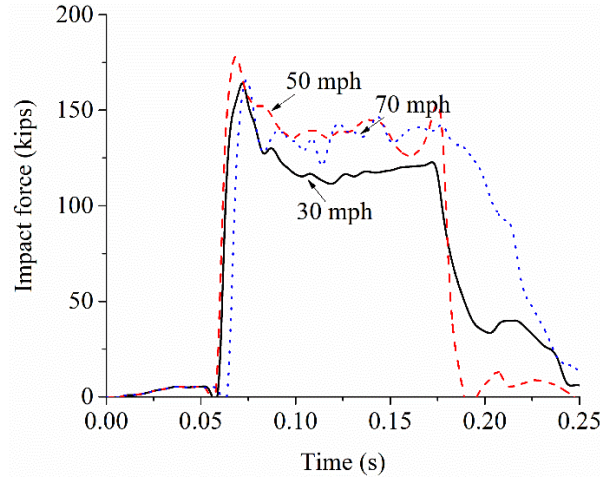


Source: FHWA

Figure 38. Graph. Crushing behavior of the honeycomb.

Figure 39 shows the impact force time histories delivered by overheight trucks at different velocities. The total weight of the truck was 40 US ton. In figure 39, the level of the impact demand was quite similar for different impact velocities from 30 mph to 70 mph. Based on the plots in figure 39, the simulated crushing force was around 125 kips, which is consistent with the design

crushing force for the honeycomb, i.e., $\sigma_{crush} \times A_{effective} = 29\text{psi} \times 4,400\text{in}^2 = 127.6 \text{ kips}$. In contrast to the short pulse demand for CFRP girder shown in figure 29, the demand for honeycomb girders shown in figure 39 was much smaller in magnitude and over a longer time, approximately 0.10 sec versus roughly 0.02 sec for the main pulse observed in CFRP demand (in figure 29).



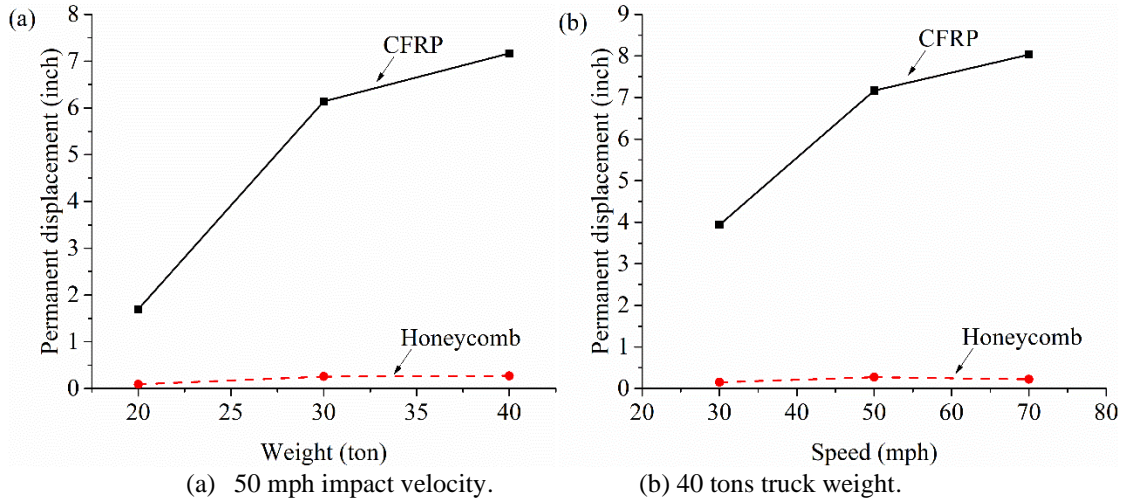
Source: FHWA

Figure 39. Graph. Impact force time history of the honeycomb beam subject to the overhead impact.

Figure 40 shows the comparison of the permanent deformation of the girder protected by CFRP wrapping (0.08-inch thickness) and honeycomb devices. In figure 40, a wide range of truck speeds and truck weights were considered. It is shown in figure 40 that the deformation of the girders protected by honeycomb was found much smaller than the CFRP wrapped girder. The deformation of the honeycomb girder was generally lower than 0.31 inch, while the CFRP girder deformation was generally larger than 1.6 inch, signifying severe damages. This is because the impact demand was well controlled by the honeycomb crushing and the crushing force was designed lower than the capacity of the girder. Figure 41 shows an example of the minor damage mode of the girder protected by honeycomb devices.

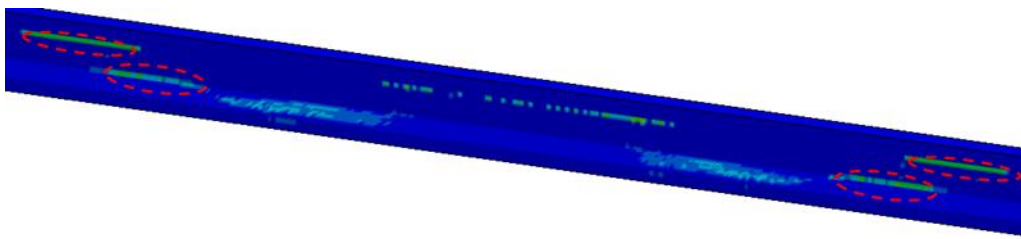
To facilitate the future design of honeycomb devices with different crushing strengths and thickness, table 6 shows the deformation energy dissipated by the honeycomb in different truck simulations and the kinetic energy of the truck. In table 6, the averaged ratio of the honeycomb energy over the kinetic energy for different cases was around 15%. In the actual design, the kinetic energy of the truck can be simply estimated by equation (7) based on the truck speed and weights.

Therefore, the averaged energy ratio shown in table 6 could be used to predict the percentage of the kinetic energy from the impacting truck that will be dissipated by the honeycombs, which can be used to design the crushing strength and honeycomb thickness to meet the design requirement based on equations (4) and (5).



Source: FHWA

Figure 40. Graph. Comparison of peak deformation of the girder protected by CFRP and honeycomb blocks.



Source: FHWA

Figure 41. Photo. Minor damage mode of bridge girder protected by the honeycomb modular.

Table 6. Computed energy of the trailer and honeycombs

Case	Trailer kinetic energy, E_k (J)	Deformation energy by the honeycomb, $E_{honeycomb}$ (J)	$E_{honeycomb} / E_k$
V30-W40	2.58×10^6	4.61×10^5	17.87%
V50-W40	7.16×10^6	1.08×10^6	15.07%
V70-W40	1.40×10^7	1.69×10^6	12.03%
V50-W20	2.63×10^6	3.20×10^5	12.18%
V50-W30	4.90×10^6	9.14×10^5	18.67%
average			15.16%

CHAPTER 5. LARGE SCALE TESTING OF A GIRDER WITH HONEYCOMB BLOCK

In this chapter, drop-hammer testing, and numerical simulations were carried out to study the impact behaviors of the innovative energy-dissipative protective beam at Hunan University, China. The main objective of this task was to further validate the material model for simulating the crashing behavior of the honeycomb and showcase the effectiveness of honeycomb in attenuating the damage in the protected member under impact load. Figure 42 shows the setup of the drop-hammer testing with the steel beam in the laboratory at Hunan University. The span length of the beam was 6.6 ft and it had a box section of 6"x6"x5/16". The size of the specimen was based on a 1:7 scale of an actual bridge girder discussed in Chapter 3. The yield strength of the steel was 50 ksi. The weight of the hammer was 2,138 lbs. For the boundary condition, the steel beam was firmly clamped at one end and free to move longitudinally at the other end. In figure 42, the bottom of the clamping devices was simply supported. Honeycomb blocks were attached to the top of the steel beam using epoxy. The crushing strength of the honeycomb was around 0.145 ksi, which was selected based on the capacity of the testing beam. (Note that this was a small-scale testing and higher crushing strength may cause damage to the protected beam.)

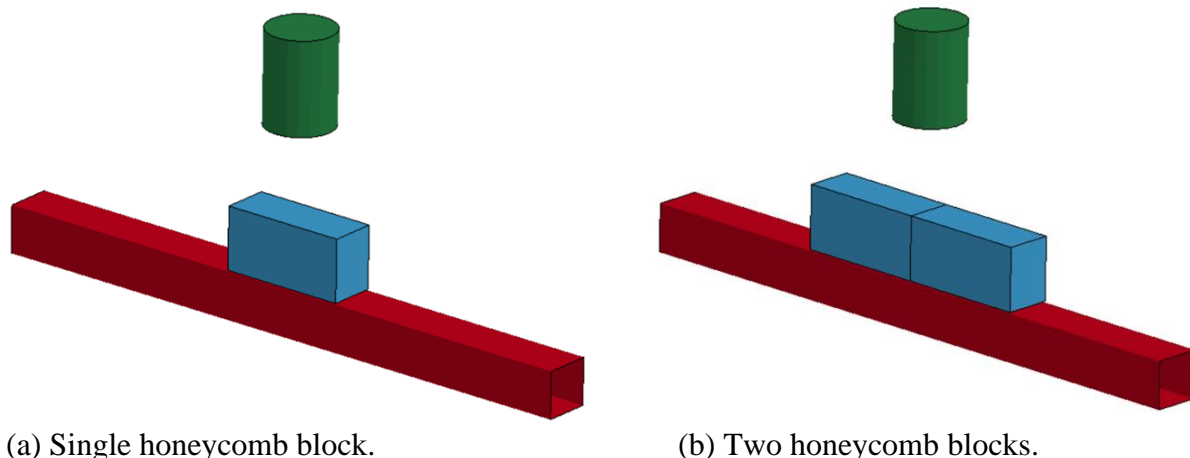


(a) Test setup of the steel beam with honeycombs. (b) Test setup showing the displacement sensor.

Source: FHWA

Figure 42. Photo. Setup of the drop-hammer test.

To study the effects of the honeycombs, six tests were carried out and are listed in table 7, where two impact speeds of 10 mph and 20 mph, were used to induce different levels of damage in the beam. For the 10-mph impact, the honeycomb thickness was 8 inches, while it was 16 inches for the 20-mph impact. For each testing speed, two configurations of the honeycomb were evaluated, which are shown in figure 43. In figure 43a, a single honeycomb with a dimension of 16-inch x 6 inch was attached to the beam and the hammer was positioned to impact the middle of the honeycomb. In figure 43b, two honeycomb blocks with the same dimensions were placed side by side on the top of the steel beam, but the two honeycomb blocks were not connected or glued to each other. For the second setup in figure 43b, the hammer will impact the middle of the two honeycomb blocks. The intent was to evaluate the crashing behavior of the honeycomb under the edge impact for each of the blocks.



Source: FHWA

Figure 43. Illustration. Two configurations of the honeycomb.

Based on the testing results, the permanent displacements of the impacted beam for each case are listed in table 7. It can be seen from table 7 that the mid-span deflection of the beam was reduced by almost 74% for the 10-mph impact and around 50% for the 20-mph impact because of honeycomb. Also, table 7 shows that the beam with a single honeycomb block had similar deformations as those protected with two honeycombs impacted at the edges.

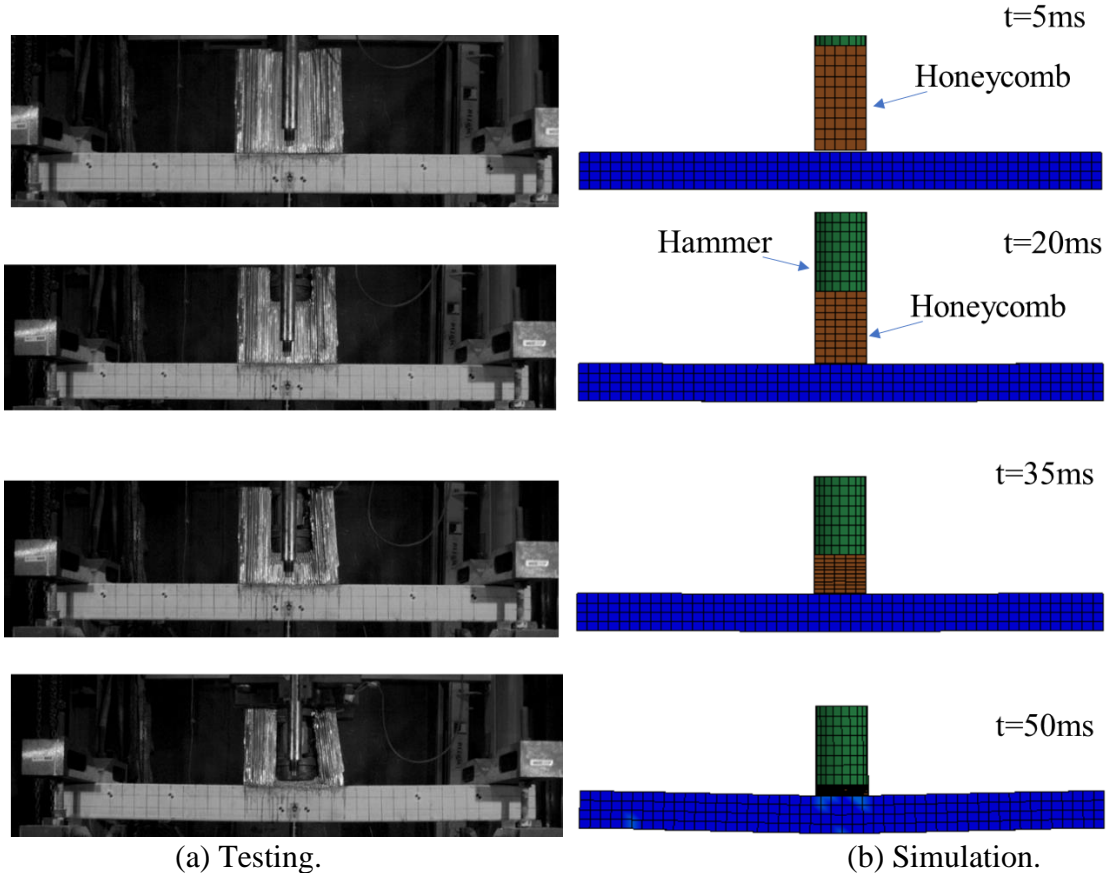
Table 7. Displacement results for each testing case

Cases	Velocity (mph)	Thickness of the honeycomb (inch)	Number of the honeycomb blocks	Permanent mid-span deflection of the beam (inch)
1	10	N/A	N/A	0.91
2	10	8	1	0.24
3	10	8	2	0.24
4	20	N/A	N/A	4.72
5	20	16	1	2.36
6	20	16	2	2.36

N/A: no honeycomb was used.

Figure 44 shows the comparison of the impact process between testing results and simulations. In the simulation model, the steel was simulated using material Mat 3 in LS-DYNA, which accounts for yielding and kinematic hardening plasticity. Shell elements were used to model the plates and were assumed to fracture and were removed after the strain reached 0.20. The general mesh size used was 1.5 inches. The honeycomb was modeled using solid element in LS-DYNA and the crushing behavior was simulated using MAT_HONEYCOMB (MAT26). Similar to the honeycomb simulation in Chapter 4, the crushing stress-strain curve for the honeycomb was based on the validation study against laboratory testing data, as illustrated in figure 36.

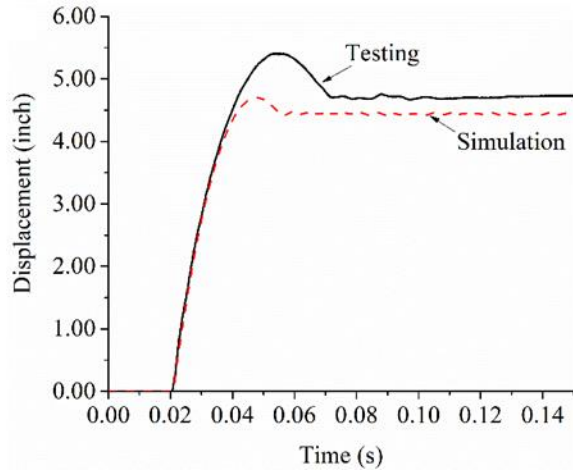
In figure 44a, it is observed that only the honeycomb block that contacted with the hammer head was crushed, while the neighboring honeycomb materials were not engaged during the impact process. Since the objective of this task was to verify the crushing behavior of the honeycombs being impacted, only the contact portion of the honeycomb was modeled in the simulation and figure 44b shows the simulated behavior of the honeycomb under the 20-mph hammer impact.



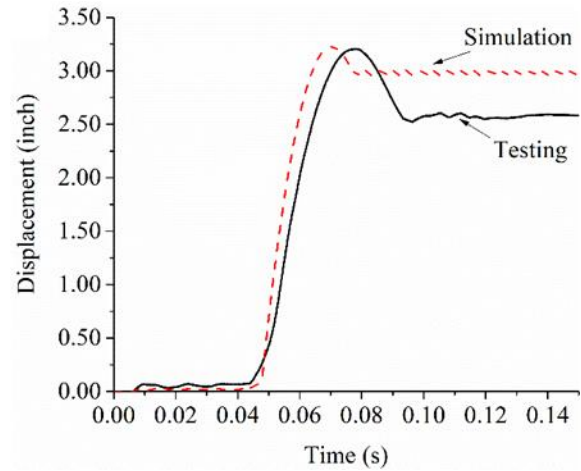
Source: FHWA

Figure 44. Photo. Impact process of the 20-mph case.

Based on the comparison in figure 44, the general crushing behavior of the honeycomb matched the testing results reasonably well. Also, figure 45 and figure 46 showed the time histories of the mid-span deflections of the beam and impact forces obtained from the testing and simulations, where good comparisons were observed. Similar good comparisons were observed in the 10-mph case, as illustrated in figure 47 and figure 48.



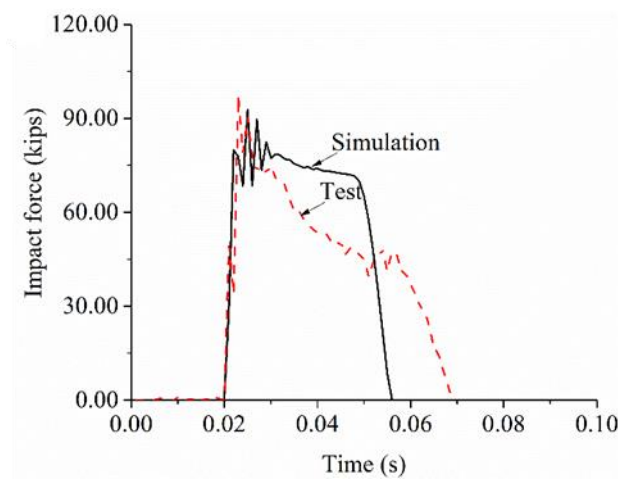
(a) Steel beam.



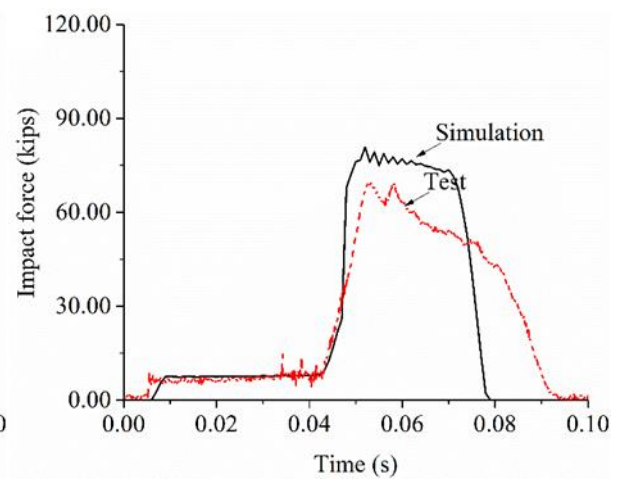
(b) Honeycomb beam.

Source: FHWA

Figure 45. Graph. Deformation time history of the beam under the 20-mph drop-hammer impact.



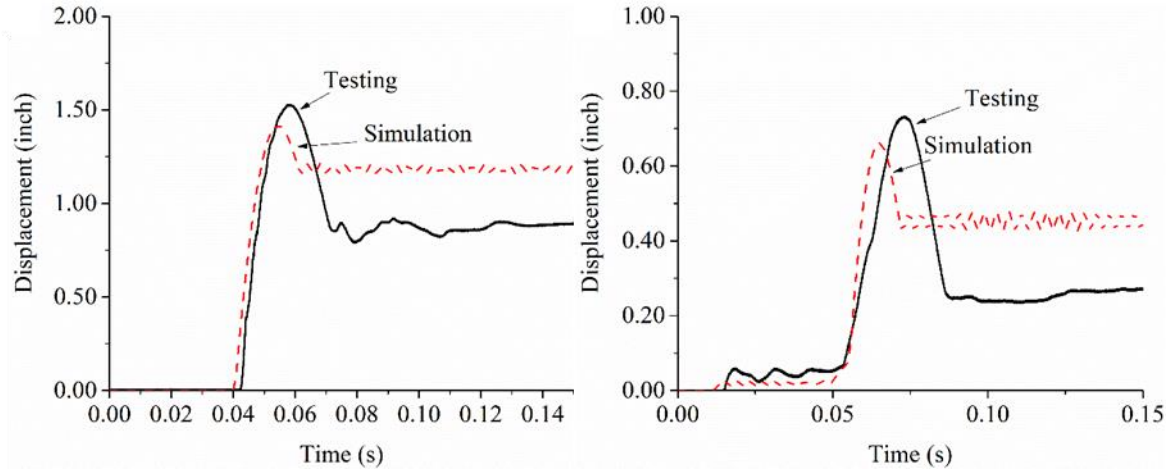
(a) Steel beam.



(b) Honeycomb beam.

Source: FHWA

Figure 46. Graph. Impact force time history of the 20-mph drop hammer impact.

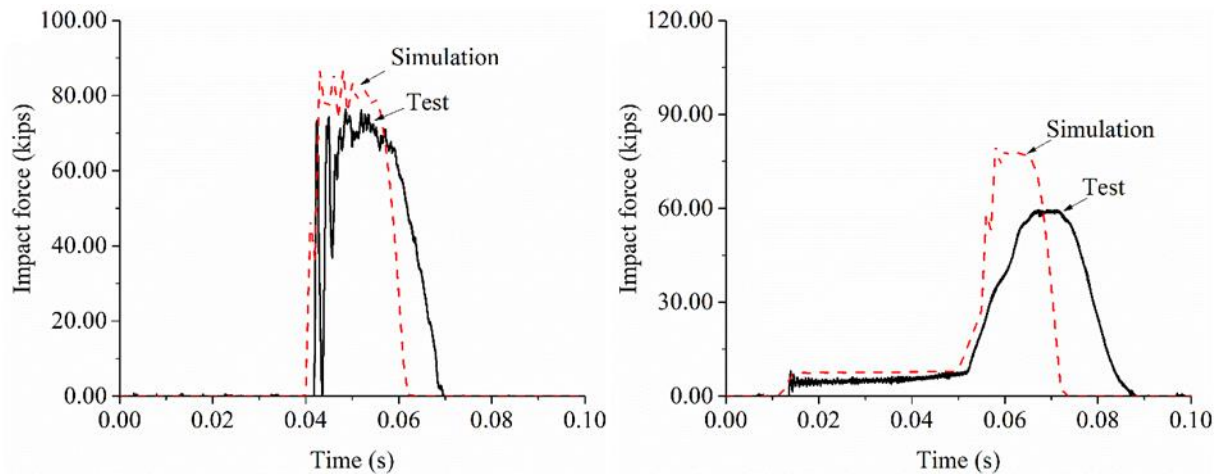


(a) Steel beam.

(b) Honeycomb beam.

Source: FHWA

Figure 47. Graph. Deformation time history of the beam under the 10-mph drop-hammer impact.



(a) Steel beam.

(b) Honeycomb beam.

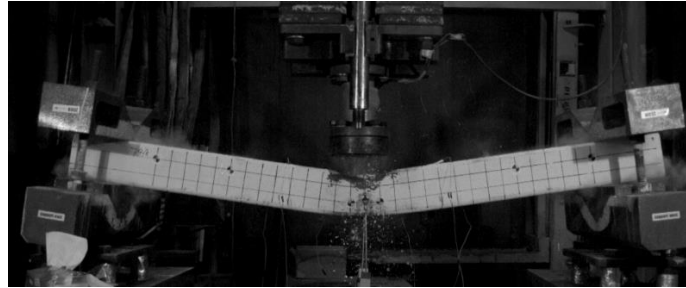
Source: FHWA

Figure 48. Graph. Impact force time history of the 10-mph drop-hammer impact.

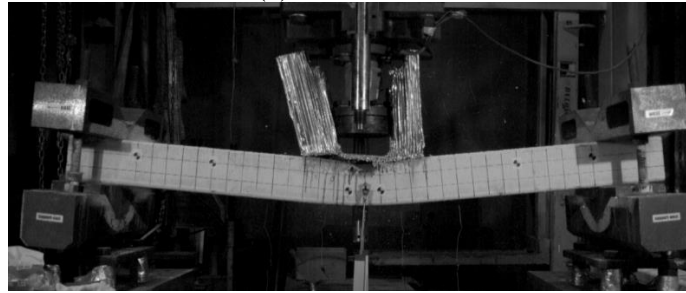
Figure 49 and figure 50 show the damage mode of the impacted beam with and without honeycombs. It can be seen from figure 49 and figure 50 that the damage extent of the beam was reduced by the honeycomb. Also, figure 51 shows the strain results at the bottom of the beam for cases with and without honeycombs. It is observed that the honeycomb reduced the permanent strain by 67% in the 10-mph case and over 50% in the 20-mph case.

To further make the honeycomb more effective in protecting the structure, the testing results indicated the need for future investigation on the design of face panel for the honeycomb to involve more honeycomb materials in resisting the impact load and in dissipating the energy. Also, the

current modeling didn't explicitly consider the shear failure of the honeycomb cells, which could be incorporated in the future to improve the accuracy of the honeycomb model.



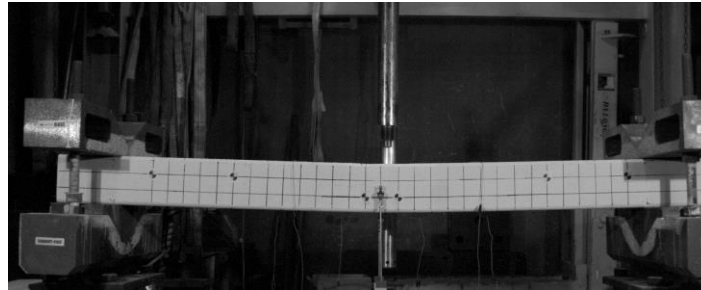
(a) Steel beam.



(b) Honeycomb beam.

Source: FHWA

Figure 49. Graph. Damage mode of the beam under 20-mph drop-hammer impact.



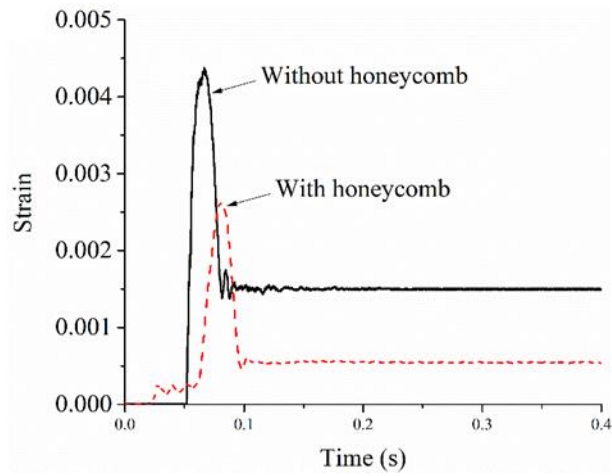
(a) Steel beam.



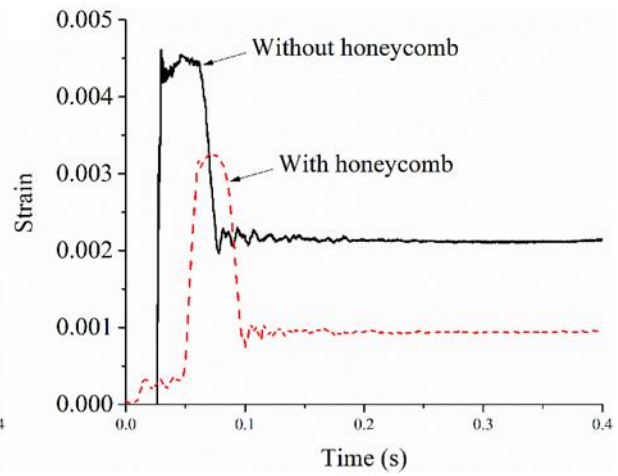
(b) Honeycomb beam.

Source: FHWA

Figure 50. Graph. Deformation mode of the beam under 10-mph drop-hammer impact.



(a) 10-mph drop-hammer impact.



(b) 20-mph drop-hammer impact.

Source: FHWA

Figure 51. Graph. Strain of the beam at point A (in figure 42).

CHAPTER 6. CONCLUSIONS, LIMITATIONS AND FUTURE WORK

SUMMARY AND CONCLUSIONS

- Based on the simulation analysis, a performance-based design framework has been proposed for the design of the steel protective beams against overheight truck impact. An equivalent pulse loading was also developed to represent the loading effects of the overheight truck at different speeds and weights.
- The effects of CFRP wrapping in protecting girders against overheight impact were evaluated using crash simulations. The simulation results showed that girders with CFRP wrapping could still be severely damaged under the overheight impact. Based on pushover simulations, it was found that the increment in the lateral capacity of the girder provided by CFRP was limited.
- Based on the simulation results, the proposed honeycomb devices were shown to be effective in reducing the impact force transmitted to the protected girders, and they could be designed to dissipate enough energy from the impacting truck so that the girder would be prevented from severe damage and the truck could be stopped.

LIMITATIONS AND FUTURE WORK

- The failure mode of debonding of CFRP sheet was not modeled in this study. More testing data are needed to simulate the debonding behavior of CFRP subject to the impact load.
- To improve the effectiveness of honeycomb devices in dissipating energy, it is recommended to investigate the design of face panels for the honeycomb cores in the future. A well-designed face panel attached to the honeycombs should be able to add more stiffness to the proposed honeycomb devices and involve more honeycombs to be crushed and not only those that are directly impacted.
- Based on the future field-testing results, the accuracy of honeycomb modeling could be further improved in future by explicitly considering the shear failure of honeycomb cells.
- Further research is recommended on the actual field installation of the honeycomb devices. Also, the combination of CFRP wrapping and honeycomb devices can be explored in the future, so that the capacity of the concrete girder can be increased and honeycombs with higher crushing strength, but small sizes can be used.
- The design of the shear plates at the ends of the protection beam should be studied. The specific design procedure of the connection details can be incorporated into the proposed performance-based design framework of the impact beam.
- A semi-rigid trailer was used in the simulations based on an actual overheight impact accident. It would be useful to collect the data of the crashing trailers, analyzing their stiffnesses, and build different levels of countermeasures in the future.

ACKNOWLEDGMENT

This material is based upon work supported by the Federal Highway Administration under contract number DTFH61-14-D-00010. This research was also partially supported by the grant from the University Transportation Research Center (UTRC). UTRC is the designated United State Department of Transportation University Transportation Center (UTC) for the federal region 2 and is housed at the City College of New York.

Any opinions, findings and conclusions or recommendations expressed in this publication are those of the author(s) and do not necessarily reflect the views of the Federal Highway Administration or the U.S. Department of Transportation.

REFERENCES

- AASHTO (2017). "AASHTO LRFD Bridge Design Specifications", American Association of State Highway and Transportation Officials, Eighth edition, Washington, D.C.
- Agrawal, A.K., El-Tawil, S., Cao, R., Xu, X., Chen, X. and Wong, W. (2018). "A Performance Based Approach for Loading Definition of Heavy Vehicle Impact Events", Federal Highway Administration, McLean, VA.
- Agrawal, A. K., Xu, X., and Chen, Z. (2011). "Bridge vehicle impact assessment." University Transportation Research Center, New York State Department of Transportation.
- Belarbi, A., Bae, S.-W., and Brancaccio, A. (2012). "Behavior of full-scale RC T-beams strengthened in shear with externally bonded FRP sheets." *Construction and Building Materials*, 32, 27-40.
- Cao, R., Agrawal, A.K., El-Tawil, S., Xu, X., and Wong, W. (2019a). " Heavy truck collision with bridge piers: a computational simulation study." *J. Bridge Eng.* 10.1061/(ASCE)BE.1943-5592.0001398
- Cao, R., Agrawal, A.K., El-Tawil, S., Xu, X., and Wong, W. (2019b). "Performance-Based Design Framework for Bridge Piers Subjected to Truck Collision." *J. Bridge Eng.*
- Cao, R., El-Tawil, S., Agrawal, A.K., Xu, X., and Wong, W. (2019c). "Behavior and design of bridge piers subjected to heavy truck collision." *J. Bridge Eng.* 10.1061/(ASCE)BE.1943-5592.0001414
- Cao, R., El-Tawil, S., Agrawal, A.K., (2019d). "Miami Pedestrian Bridge Collapse: A Computational Forensic Analysis" *J. Bridge Eng.* ASCE. DOI: 10.1061/(ASCE)BE.1943-5592.0001532
- Cao, R., Agrawal, A.K., El-Tawil, S., and Wong, W. (2020a). "Overheight Impact on Bridges: A Computational Case Study of the Skagit River Bridge Collapse". *Eng. Struct.* (under review).
- Cao, R., Agrawal, A.K., El-Tawil, S., and Wong, W. (2020b). "Numerical studies on Concrete Barriers Subjected to MASH Truck Impact". *J. Bridge Eng.* 10.1061/(ASCE)BE.1943-5592.0001570.
- Do, T. V., Pham, T. M., and Hao, H. (2018). "Numerical investigation of the behavior of precast concrete segmental columns subjected to vehicle collision." *Engineering Structures*, 156, 375-393.
- Hallquist, J. O. (2006). "LS-DYNA theory manual." *Livermore software technology corporation*, 3, 25-31.
- Jiang, H., and Chorzepa, M. G. (2015). "An effective numerical simulation methodology to predict the impact response of pre-stressed concrete members." *Engineering Failure Analysis*, 55, 63-78.
- Liu, G., (2012). "Behavior of Bridge Piers during Vehicular Impacts." Ph.D thesis, City College of New York, City University of New York.
- Miele, C. R., Plaxico, C., Stephens, D., and Simunovic, S. (2010). "U26: Enhanced Finite Element Analysis Crash Model of Tractor-Trailers (Phase C)."
- Moutoussamy, L., Herve, G., and Barbier, F. (2011). "Qualification of *Constrained_Lagrange_In_Solid command for steel/concrete interface modeling." *Proc., Proceedings of the 8th European LS-Dyna Conference.*

- Murray, Y. D., Abu-Odeh, A. Y., and Bligh, R. P. (2007). "Evaluation of LS-DYNA concrete material model 159." FHWA-HRT-05-063, Federal Highway Administration, McLean, VA.
- Nakalswamy, K. K. (2010). "Experimental and numerical analysis of structures with bolted joints subjected to impact load." Ph.D. thesis, University of Nevada, Las Vegas.
- NTSB (National Transportation Safety Board). (2014). "Collapse of the Interstate 5 Skagit River bridge following a strike by an oversize combination vehicle, Mount Vernon, Washington, May 23, 2014." Accident Rep. NTSB/HAR-14/01, Washington, DC.
- Plaxico, C., Miele, C., Kennedy, J., Simunovic, S. and Zisi, N., Enhanced Finite Element Analysis Crash Model of Tractor-Trailers (Phase A), National Transportation Research Center, Inc., Knoxville, TN (2008).
- Plaxico, C., Miele, C., Kennedy, J., Simunovic, S. and Zisi, N., Enhanced Finite Element Analysis Crash Model of Tractor-Trailers (Phase B), National Transportation Research Center, Inc., Knoxville, TN (August 2009).
- Qiao, P., Yang, M., Mosallam, A. and Song, G. (2008). An overheight collision protection system of sandwich polymer composites integrated with remote monitoring for concrete bridge girders (No. FHWA/OH-2008/6). University of Akron. Dept. of Civil Engineering.
- Rosenboom, O., Walter, C., and Rizkalla, S. (2009). "Strengthening of prestressed concrete girders with composites: Installation, design and inspection." *Construction and Building Materials*, 23(4), 1495-1507.
- Ross Jr, H., Sicking, D., Zimmer, R., and Michie, J. (1993). "Recommended procedures for the safety performance evaluation of highway features (NCHRP Report 350). Washington, DC: Transportation Research Board."
- Xu, X., Cao, R., El-Tawil, S., Agrawal, A.K. and Wong, W. (2019). " Loading definition and design of bridge piers impacted by medium weight trucks." *J. Bridge Eng.* 10.1061/(ASCE)BE.1943-5592.0001397
- Zimmerman, R. (2012). *Transport, the Environment and Security: Making the Connection*, Edward Elgar Publishing.